# Quantifying watershed sensitivity to spatially variable N loading and the relative importance of watershed N retention mechanisms

Kristin K. Gardner,[1] Brian L. McGlynn,[1] and Lucy A. Marshall[1]

Received 9 July 2010; revised 6 June 2011; accepted 22 June 2011; published 20 August 2011.

[1] The link between watershed nitrogen (N) loading and watershed nitrate ($NO_3^-$) export is poorly understood yet critical to addressing the growing global problem of watershed N enrichment. We introduce the Big Sky nutrient export model (BiSN) which incorporates spatial stream water chemistry, data from instream tracer additions and geologic weathering experiments, and terrain and land use analysis to quantify the spatial variability of watershed sensitivity to N loading and the relative importance of upland, riparian, and instream N retention (storage, removal, or transformation) across land use/land cover (LULC) and landscape positions. Bayesian Markov chain Monte Carlo (MCMC) methods were used for model specification and were helpful in assessing model and parameter uncertainty and advancing understanding of the primary processes governing watershed $NO_3^-$ export. Modeling results revealed that small amounts of wastewater loading occurring in watershed areas with short travel times to the stream had disproportionately large impacts on watershed nitrate ($NO_3^-$) export compared to spatially distributed N loading or localized N loading in watershed areas with longer travel times. In contrast, spatially distributed N inputs of greater magnitude (terrestrial storage release and septic systems) had little influence on $NO_3^-$ export. During summer base flow conditions, 98%–99% of watershed N retention occurred in the uplands, most likely from biological assimilation or lack of hydrologic transport. The relative role of instream N retention increased with N loading downstream through the stream network. This work demonstrates the importance of characterizing the spatial variability of watershed N loading, export and retention mechanisms, and considering landscape position of N sources to effectively manage watershed N.

**Citation:** Gardner, K. K., B. L. McGlynn, and L. A. Marshall (2011), Quantifying watershed sensitivity to spatially variable N loading and the relative importance of watershed N retention mechanisms, *Water Resour. Res., 47*, W08524, doi:10.1029/2010WR009738.

## 1. Introduction

[2] Human activities have greatly increased the bioavailability of nitrogen (N), primarily from the addition of fertilizers, human and animal waste, and the burning of fossil fuels [*Vitousek et al.*, 1997]. With increasing amounts of bioavailable N, biotic demand can become saturated, potentially resulting in excess N delivered to surface waters [*Aber et al.*, 1989]. N enrichment of aquatic resources can have profound impacts on ecosystem function by stimulating primary production which can alter biological communities and expedite eutrophication [*Allen*, 1995].

[3] Minimizing the influence of anthropogenic N on aquatic ecosystems is one of watershed management's biggest challenges. This is because the relationship between anthropogenic N loading and stream N export is complicated; N is not conservatively transported and there is potential for N retention to occur in terrestrial and stream ecosystems. For the purpose of this paper, we define retention as physical, biological, or chemical processes that temporarily or permanently inhibit downstream transport of N. Mechanisms for N retention include: (1) microbial denitrification [*Brooks et al.*, 1996; *Burt et al.*, 1999], (2) plant or microbial assimilation [*Hadas*, 1992; *Nadelhoffer et al.*, 1999], (3) physical sorption [*Qualls and Haines*, 1992; *Triska et al.*, 1994], (4) biotic and abiotic retention through iron [*Davidson et al.*, 2003] and sulfur reduction [*Brunet and Garcia-Gil*, 1996], and (5) fermentative nitrate reduction [*Tiedje*, 1988]. N retention can alter the timing, magnitude, and form of N transported creating complex spatial and temporal patterns in stream water N.

[4] For effective management of stream water N, it is critical to identify and quantify the spatial distribution of watershed N loading and retention. For this, environmental managers often rely upon water quality models. A water quality model is a set of equations that can be used to describe the processes that determine instream N concentrations or loads. Models of watershed N export range in their complexity from simple empirical models with minimal data requirements to complex mechanistic models that require enormous amounts of data. For a review of watershed N export models and their range of complexity see *Alexander et al.* [2002]. Selecting the level of model complexity should depend on the (1) goals or objectives of the model, (2) available data, (3) computational efficiency,

[1]Department of Land Resources and Environmental Sciences, Montana State University, Bozeman, Montana 59717, USA.


0043-1397/11/2010WR009738

(4) budgetary constraints [*U.S EPA*, 1976], (5) spatial scale [*Soulsby et al.*, 2006], and (6) level of predictive uncertainty [*Perrin et al.*, 2001].

[5] Overly complex models typically "upscale" physical process knowledge from plot scale experiments, which may not be appropriate at the watershed scale [*Kirchner*, 2006] and can lead to problems of over parameterization and equifinality [*Beven*, 1993, 2006] that in turn may result in large predictive uncertainty. High predictive uncertainty is common in water quality applications as a result of spatial variability of environmental variables, parameter uncertainty, measurement error, and conceptual uncertainty [*Beven*, 2001]. Simple watershed models are an attractive approach to reduce predictive uncertainty and can be suitable for some watersheds processes like describing an integrated watershed response [*Savenije*, 2001]. Ideally, a model should have a small number of parameters with a high enough level of mechanistic detail to represent the major processes controlling the modeled phenomena or the model may lead to misrepresentative conclusions and poor land management decisions [*Young et al.*, 1996].

[6] Export coefficient models represent a relatively simple modeling approach that has been applied in many catchments to predict nutrient loads and has been shown to be capable of accurately simulating nutrient export [*Reckhow and Simpson*, 1980; *Beaulac and Reckhow*, 1982; *Rast and Lee*, 1983; *Johnes*, 1996; *Worrall and Burt*, 1999; *McFarland and Hauck*, 2001; *Zobrist and Reichert*, 2006]. The basic export coefficient model assumes that land use is a major driver of catchment nutrient export. These models calibrate nutrient export coefficients, which represent the amount of nitrogen or phosphorus exported from a specific land use over a specific time period. Several studies have introduced process representation into the basic export coefficient model by adding (1) export coefficients weighted within a threshold distance (50 m) from rivers [*Johnes and Heathwaite*, 1997], (2) soil nitrogen reserves [*Worrall and Burt*, 1999], (3) present and previous year rainfall to weight N loss from soil nitrogen reserves and a nondescript buffering capacity proportional to the amount of N released [*Worrall and Burt*, 2001], (4) monthly runoff data to capture seasonal variability in phosphorous export [*Hanrahan et al.*, 2001], (5) export coefficients weighted by the topographic index representing potential for phosphorous transport and a buffer index, based on land cover average slope to predict retention of overland runoff [*Endreny and Wood*, 2003], and (6) an erosion index as a surrogate for hydrologic variability in modeling phosphorus export [*Khadam and Kaluarachchi*, 2004].

[7] This paper introduces the Big Sky Nitrogen Export model (BiSN) which predicts watershed nitrate ($NO_3^-$) export by incorporating terrestrial and instream retention process representation into a basic export coefficient model. The spatial structure of BiSN allows for determination of the relative magnitudes of watershed N loading, and terrestrial and instream retention across the stream network, which can vary significantly because of spatial heterogeneous nature of mountain environments [*Seastedt et al.*, 2004] and resort development [*Campos et al.*, 2010]. BiSN's approach can provide valuable insight for land managers to aid in development of effective land use planning that addresses the spatial variability of N dynamics occurring within a catchment or for researchers to formulate more focused research questions to gain process knowledge. We consider the uncertainty in the BiSN output and its parameters by applying a Bayesian Markov chain Monte Carlo (MCMC) approach.

[8] We applied BiSN to summer synoptic stream water $NO_3^-$ data collected in a developing mountain watershed to (1) determine the model's ability to characterize the spatial heterogeneity of stream water $NO_3^-$ export, (2) identify the primary drivers of stream water $NO_3^-$ export and how they may vary across LULC and landscape position, and (3) quantify the spatial distribution of N loading and retention and $NO_3^-$ export along the stream network.

## 2. Study Area

[9] The West Fork of the Gallatin River in the northern Rocky Mountains of southwestern Montana (Figure 1A) drains Big Sky, Moonlight Basin, Yellowstone Club, and Spanish Peaks resort areas (Figure 1B). The West Fork watershed (212 $km^2$) is characterized by steep topography and shallow soils. Elevation in the drainage ranges from approximately 1800 to 3400 m and average annual precipitation exceeds 1270 mm at higher elevations and is less than 500 mm near the watershed outlet. Sixty percent of precipitation falls during the winter and spring months [*USDA NRCS*, 2008]. Hydrographs of the West Fork River indicate peak flows during spring snowmelt typically occurring in late May and early June followed by a general recession throughout the summer, autumn, and winter months.

[10] Streams in the West Fork watershed range from first-order, high gradient, boulder dominated mountain streams in the upper elevations to fourth-order, alluvial streams near the watershed outlet. Stream productivity is generally low due to cold temperatures and short growing seasons [*USDA FS*, 2004], however in recent years, increased algal growth has been noted in streams draining developed subwatersheds near the watershed outlet. The increased algal growth in streams draining development may be signs of the beginning stages of N enrichment. Chlorophyll-a data collected in September 2005 suggest that algal growth was elevated above natural background levels in streams draining developed subwatersheds. Median Chlorophyll-a measurements from scraped rocks ranged from 2.5 mg $m^{-2}$ in pristine low order streams, 20 mg $m^{-2}$ in pristine higher order streams, to 360 mg $m^{-2}$ in higher order streams draining more developed watersheds [*PBS&J*, 2005].

[11] Diverse geologic materials are present in the West Fork watershed, including metamorphosed volcanics of Archean age, sedimentary and meta-sedimentary formations of various ages, and colluvium and glacial deposits that dominate the surficial geology in valley bottoms. Carbonaceous rocks such as limestones and shales are present in some but not all headwater catchments, and quartzite, biotite, gneiss, gabbros, and sandstones are also present [*Alt and Hyndman*, 1986; *Kellog and Williams*, 2006]. Vegetation below tree line consists of coniferous forest (lodgepole pine, blue and Engelmann spruce, and Douglas fir), grasslands, shrublands, and willow and aspen groves in the riparian areas. The watershed has a brief growing season from mid-June through mid-September (75–90 frost free days), decreasing with elevation [*USDA FS*, 1994].

[12] Big Sky Resort was established in the early 1970s and since then, the West Fork watershed has seen a rapid

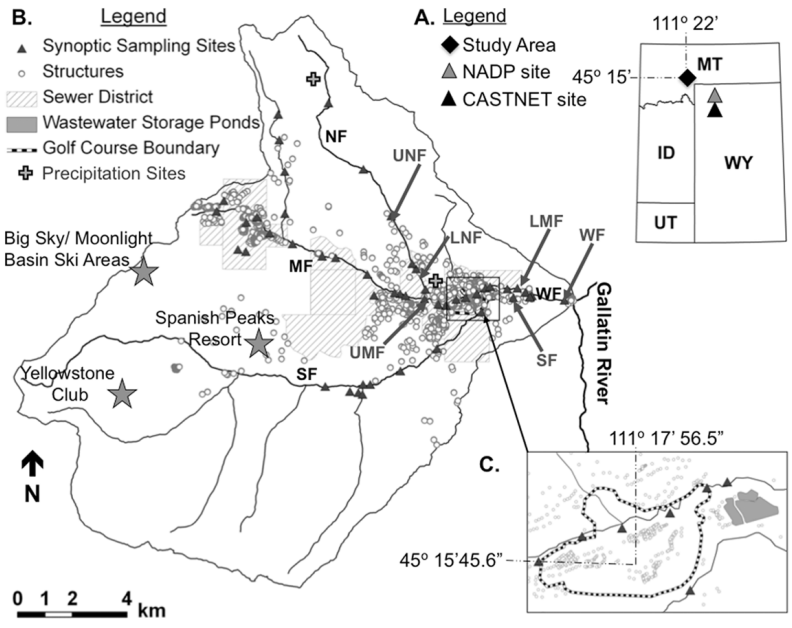


**Figure 1.** (A) Location of the West Fork watershed (212 km$^2$) in southwestern Montana, with locations of atmospheric wet (NADP) and dry (CASTNET) deposition data collection sites. (B) Map of the West Fork watershed showing locations of 50 synoptic sampling sites (black triangles), building structures (gray circles), precipitation gauges (gray crosses), and the Big Sky Water and Sewer District boundaries (gray hatched lines). The West Fork (WF) drains into the Gallatin River (a tributary of the upper Missouri River) and is composed of three main tributaries: the Middle Fork (MF), the North Fork (NF), and the South Fork (SF). (C) An expanded view of the wastewater storage ponds and the Big Sky Resort Golf Course. Wastewater effluent is stored in the ponds and irrigated onto the golf course from mid-May through early October.

increase in growth with the addition of three new ski resorts and golf courses with associated residential development. Since resort development, annual average stream water $NO_3^-$ concentrations in the West Fork of the Gallatin River have followed a similar upward trend as development, represented by the number of building structures in the 212 km$^2$ watershed (Figure 2). This historical data, collected at the catchment outlet, was the impetus for further exploration of the spatial and seasonal variability of N loading, retention, and export occurring within the West Fork watershed and their controls on catchment response.

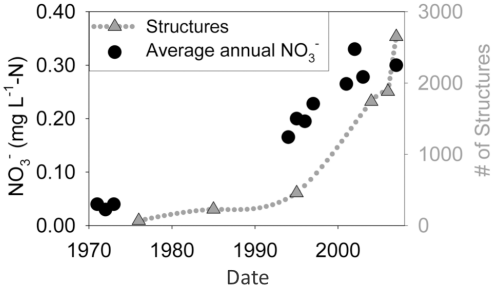


**Figure 2.** In the West Fork watershed, residential development and annual average stream water $NO_3^-$ concentrations have followed a similar upward trend since resort development. [*NSF*, 1976; *Blue Water Task Force, and Big Sky Water and Sewer District*, unpublished data].

[13] Sources of nitrogen within the West Fork watershed include: atmospheric deposition, N fixation, fertilizer, pet waste, and wastewater (septic and public sewer disposal). The Big Sky Water and Sewer District services the two village areas with public water supply and sewer in the West Fork watershed (Figure 1B). Public wastewater receives secondary treatment and is released into three lined sewer detention ponds and stored until midspring when it is released as irrigation water onto the Big Sky Golf Course (Figure 1C). Golf course irrigation begins in midspring when the ground thaws and continues through midfall, when the ground again freezes. Areas outside of the sewer district are on individual or community septic systems and private wells [*Edwards*, personal communication, 2007].

## 3. Methods

[14] The BiSN model uses a traditional export coefficient modeling approach, which assumes nutrient export is purely a function of land use export [*Reckhow and Simpson*, 1980; *Johnes*, 1996], but additionally incorporates spatially explicit observations of land and stream attributes. The BISN modeling framework then allows for representation of spatially distributed N processes while retaining relative model parsimony. We describe here the data collection and construction of BiSN. Model inputs included (1) field data collected to describe the spatial variability in stream water $NO_3^-$, instream $NO_3^-$ retention, atmospheric inorganic N deposition, and stream discharge, (2) laboratory experiments to estimate the potential for mineral release of

total dissolved N (TDN), (3) terrain indices associated with rates of transport through the watershed and with riparian buffering potential, and (4) land use/land cover acting as principal sources or sinks of watershed N.

### 3.1. Stream Water Sampling and Chemistry Analysis

[15] The spatial distribution of watershed $NO_3^-$ export was measured through a synoptic, or "snapshot-in-time," sampling in which stream water was collected 8 August 2007 in 250 mL high-density polyethylene (HDPE) bottles from 50 sites across the West Fork watershed within 2–3 h time (Figure 1B). Synoptic sampling sites were selected to represent a range of subwatershed characteristics including: land use/land cover (LULC), number of wastewater disposal units, geology, stream order, elevation, and discharge (Figure 1B). This study focuses on summer $NO_3^-$ export for the following reasons: (1) there was adequate summer instream $NO_3^-$ retention data to formulate a relationship between $NO_3^-$ retention and watershed characteristics and (2) BiSN's results were employed for total maximum daily load development, which in Montana is primarily concerned with summer low flow conditions. We recognize that summer conditions may not represent the full range of system response; however, previous work has shown seasonal variability in LULC's influence on stream water $NO_3^-$ [*Gardner and McGlynn*, 2009] suggesting value in examining the drivers of $NO_3^-$ export for a single season.

[16] Instream tracer experiments using both conservative chloride and biologically active $NO_3^-$ tracers were conducted in six stream reaches representing a range of watershed and land use characteristics [*McNamara*, 2010]. Two tracer addition methods were followed: constant-rate tracer additions using modified methods from *Webster and Valett* [2006] and instantaneous tracer additions using the newly developed TASCC method (tracer additions for spiraling curve characterization) accomplished as part of this project and related research by the MSU Watershed Hydrology Laboratory [*Covino et al.*, 2010a, 2010b]. N, chloride, and specific conductance data collected during the tracer addition experiments were used to estimate total $NO_3^-$ removed from the water column (retention + removal), Michaelis-Menten kinetic model parameters (including ambient retention), and spiraling parameters for each of six stream reaches. Variability among stream reaches was found to be a function of watershed area, $NO_3^-$ concentration, and season [*McNamara*, 2010; *Covino et al.*, 2010a].

[17] Continuous stage data was collected at four locations on the West Fork and its three tributaries [*PBS&J*, 2008]. Stream discharge was calculated from stage-discharge rating curves developed from measurements over the full range of discharge. Discharge was determined with a Marsh McBirney Flo-Mate 2000™ current velocity meter and the standard USGS area-velocity method. During the summer base flow period, the relationship between watershed area and stream discharge measured at four locations on the West Fork and its three main tributaries was strongly correlated ($R^2 = 0.99$) and significant ($p < 0.05$). For reaches in which no discharge data was collected, this regression relationship was used to scale discharge.

[18] Stream water samples from the synoptic campaigns and the tracer additions were chilled to 0–4 °C and transported to the laboratory where they were filtered within 24 h of collection with 0.45 μm millipore isopore polycarbonate membranes. Filtered water samples were preserved in HDPE bottles and frozen until analysis. Dissolved aqueous nitrogen species analyzed included nitrite ($NO_2^-$), $NO_3^-$, ammonium ($NH_4^+$), and organic N. For this study we chose to examine inorganic N (for more details on organic N, see K. K. Gardner and B. L. McGlynn, Multi-analysis approach to assess the spatio-temporal patterns of watershed response to localized inputs of anthropogenic nitrogen, manuscript in preparation, [2011]), but since most samples contained $NO_2^-$ and $NH_4^+$ levels near or below detection limits (0.005–0.01 mg $L^{-1}$), we focused on $NO_3^-$. $NO_3^-$ was analyzed by ion-exchange chromatography (IC) using a Metrohm Peak model 820 interface equipped with a 4 mm anion-exchange column (Metrohm, Herisau, Switzerland). The detection limit for $NO_3^-$ was 0.01 mg $L^{-1}$−N, accuracy was within 10% for certified 0.09 mg $L^{-1}$ $NO_3^-$−N standards (0.09 ± 0.009 mg $L^{-1}$−N), as measured every 11th sample. Coefficients of variation (CVs) for $NO_3^-$ standard peak areas were 2% or less.

### 3.2. Terrestrial Sources of N

[19] Terrestrial storage of N occurs from plant and microbial immobilization, soil adsorption, and the accrual of N loading from atmospheric deposition, chemical weathering, fixation, and human and animal waste. The release of inorganic N from terrestrial storage is the summation of a number of processes including mineralization, nitrification, mineral weathering, and dissolution. These processes were subsumed in the terrestrial storage release variable in BiSN, $b_{tsr}$. While the terrestrial storage of N was not partitioned into its accumulation processes, the spatial variability of relative mineral weathering inputs across the landscape was estimated from N produced in laboratory rock weathering experiments (G. Ackerman-Montross et al., Nitrogen production from geochemical weathering of rocks in Southwest Montana, USA, manuscript in preparation, 2011). Supporting previous research suggesting geology can be a substantial source of watershed N [*Holloway et al.*, 1998, 2001], Ackerman-Montross et al. (manuscript in preparation, 2011) found a wide range of N produced from incubations of rock flour slurries from geologic materials collected across the West Fork Watershed. After 70 h of rock-water slurry incubation, 0.06 to 13.9 mg per kg rock flour was produced (solid:liquid ratio = 1.8) from eight rock types. The maximum TDN was collected from a Cretaceous limestone (Kootenai Formation) rock-water slurry (13.9 mg N per kg rock) found in 9% of the West Fork Watershed (Ackerman-Montross et al., manuscript in preparation, 2011). This production is likely much greater than under natural conditions, and therefore these results only partially informed relative weighting of N released from terrestrial storage. Watershed areas overlying bedrock geology of Cretaceous carbonates of the Kootenai Formation were assumed to release 10 times more N than watershed areas overlying other types of geology; therefore, in BiSN, the $b_{tsr}$ value in grid cells with geology less prone to weather inorganic N (91% of the grid cells) was multiplied by 0.1.

### 3.3. Atmospheric Deposition

[20] Inputs of inorganic N ($NO_3^-$ and $NH_4^+$), from atmospheric dry and wet deposition can be a significant

source of watershed N loading [*Aber et al.*, 1989; *Burns*, 2003]. The atmospheric dry deposition inorganic N load was assumed equivalent to the average dry deposition inorganic N load measured between 2000 and 2007 in the northwestern corner of Yellowstone National Park (Figure 1A) [*US EPA CMAD*, 2009]. This site, located at 2400 m and 100 km from the West Fork watershed, had no discernable temporal trend in inorganic N deposition across this time period. Atmospheric dry deposition inorganic N load was assumed to be constant across the study area. The atmospheric wet deposition inorganic N load was computed from average wet deposition inorganic N concentrations measured at Tower Falls in Yellowstone National Park between 2000 and 2007, when there was no observed trend in inorganic N concentration. (Figure 1A) [*NADP*, 2010]. Tower Falls, which is 40 km north of the dry deposition site in Yellowstone National Park at 1900 m and 70 km southeast of the West Fork watershed, was presumed to have similar wet N deposition as lower elevations of the West Fork. We assumed that N concentration in wet deposition was constant across the West Fork but the load varied by elevation because of precipitation differences [*Lovett et al.*, 1997; *Lawrence et al.*, 2000]. Consequently, the atmospheric wet deposition load for each modeled grid cell in the study area was calculated by multiplying inorganic N concentration by elevation scaled precipitation. Elevation scaled precipitation was determined by a statistical relationship developed between precipitation and elevation data from two weather stations in the study area (Appendix A): (1) the Lone Mountain SNOTEL station located in the headwaters of the North Fork watershed (Figure 1B) at 2706 m in a subalpine environment and (2) the Lone Mountain Ranch weather station, located toward the valley bottom at 2100 m.

### 3.4. Watershed Characteristics

#### 3.4.1. Terrain Analysis

[21] Landscape characteristics partially control hydrologic flow paths [*Dunne*, 1978; *Newson*, 1997] and therefore, watershed $NO_3^-$ transport. Definition of hydrological flow paths, potential travel times along each flow path, and the concomitant spatial pattern of N loading across the West Fork watershed are necessary to explain variability in stream water $NO_3^-$. To explicitly characterize the spatial distribution of N loading by various sources, the BiSN model includes the discretization of the landscape to units representing different hydrologic and land use conditions.

[22] The West Fork watershed has steep slopes and predominately thin soils with high hydraulic conductivities [*USDA SCS*, 1978, 1982]. These conditions often promote shallow subsurface runoff pathways that can result in rapid $NO_3^-$ delivery to riparian zones and streams. Consequently, hydrological flow paths are likely to be well represented by surface topography. For this study, the MD$\infty$ flow accumulation algorithm [*Seibert and McGlynn*, 2007] was used to define the hydrological flow paths and extract relevant terrain characteristics to model stream water $NO_3^-$ concentrations. First, an approximation of water transit time for each grid cell was calculated [*McGuire et al.*, 2005] and referred to as water travel time (*TT*) (for more details, see *Gardner and McGlynn* [2009]). $NO_3^-$ retention and/or removal have been shown to be inversely related to water residence time in lakes, rivers [*Seitzinger et al.*, 2002], and groundwater [*Bohlke and Denver*, 1995].

[23] In addition to *TT*, a riparian buffering index (*RBI*) was computed by an automated method in which the delineated riparian zone area associated with each stream pixel is divided by the local contributing area (lateral upslope inflows) [*McGlynn and Seibert*, 2003; *Jencso et al.*, 2010; *Grabs et al.*, 2010] (for more details see *Gardner and McGlynn* [2009]). Stream reach to stream reach assessment of riparian buffering potential of lateral hillslope inputs is pertinent in LULC change-water quality analyses because it allows for assessment of potential riparian buffering downgradient (along each flow path) of $NO_3^-$ inputs.

[24] The stream network was delineated into reaches approximately 500 m in length. A total of 231 nested subwatersheds were delineated, ranging in area from 0.01 to 207 $km^2$. Upstream subwatersheds were subtracted from downstream subwatersheds to create nonnested subwatersheds so that each land pixel contributed to only 1 stream reach. Nonnested subwatersheds ranged in area from 0.01 to 3.7 $km^2$ (Figure 3A).

#### 3.4.2. Land Cover Analysis

[25] LULC was delineated from a cloud-free QuickBird 2.4 m multispectral imagery scene acquired on 21 July 2005 combined with 1 m airborne laser swath mapping data using object-oriented classification [*Campos et al.*, 2010] for input into BiSN. Delineated land use classes included forest, impervious surface, grass, golf, soil, and sewer ponds. Septic locations were mapped by masking the Big Sky Water and Sewer District boundary GIS layer over a 2006 structure layer supplied by the Gallatin County Planning District. Geologic maps, acquired from the Montana Bureau of Mines and Geology [*Kellog and Williams*, 2005] were used to determine the percent geology with higher potential for N weathering in each reach contributing area (Ackerman-Montross et al., manuscript in preparation, 2011). LULC and terrain characteristics were then extracted as variables in BiSN.

[26] The model parameters identified from LULC and terrain analysis included forest, impervious surface, grass, golf, soil, septic, sewer ponds, geology, riparian buffer, and relative travel time. Since initial model simulations resulted in poor convergence and high parameter correlations, model parameter classes were lumped [*Bates and Campbell et al.*, 2001] so that "vegetation" consisted of grass and forest, "nonvegetation" consisted of impervious surface and soil, and "wastewater" consisted of the golf courses and sewer ponds. Additional model simulations demonstrated that $NO_3^-$ export was insensitive to the nonvegetation parameter illustrated by a uniform posterior distribution across the entire prior distribution. Furthermore, the nonvegetation Markov chain did not converge despite relatively long model runs and low correlations with other parameters. For these reasons, the nonvegetation parameter was not included in the final model. The insensitivity of nonvegetation parameter suggests that nonvegetation was not a primary driver of stream water concentrations during the summer growing season. Other research has shown impervious surface to be most associated with watershed $NO_3^-$ export during high runoff events [*Lunetta et al.*, 2005; *Shields et al.*, 2008], while having less influence on watershed $NO_3^-$ export during drier periods [*Lunetta et al.*, 2005]. In addition, impervious surface has been shown to exhibit threshold behavior in its influence

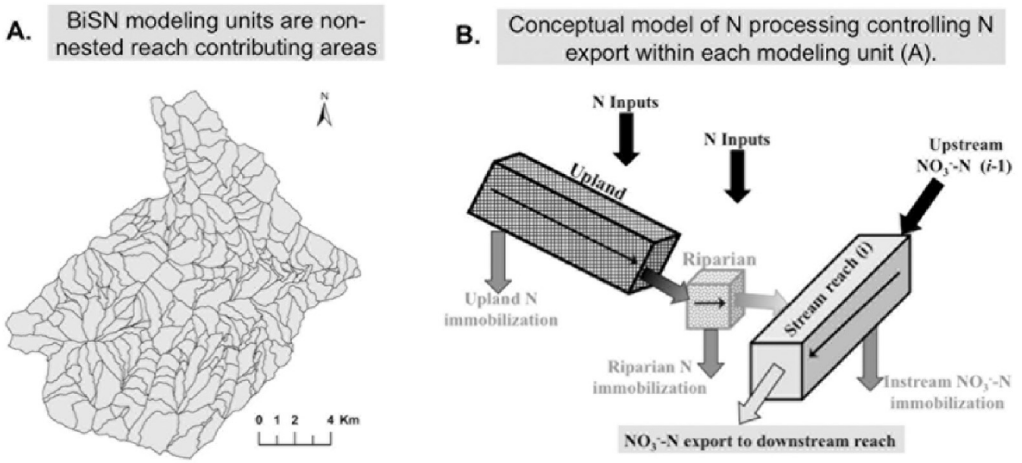


**Figure 3.** (A) Watershed modeling units of the Big Sky nutrient model (BiSN) were 231 nonnested stream reach contributing areas ranging in size from 0.01 to 3.7 km$^2$. The stream network was delineated into stream reaches of approximately 500 m in length. A 500 m stream reach length was chosen because 97% of measured $NO_3^-$ uptake lengths were less than 500 m [McNamara, 2010]. (B) Conceptual model of processes controlling N loading and retention West Fork watershed. Stream reach $NO_3^-$ is as function of upstream $NO_3^-$ inputs and lateral loading from the reach contributing area (A). N can be immobilized instream and in the upland and riparian areas as it travels along hydrological flow paths to the stream.

on watershed $NO_3^-$ export [*Carle et al.*, 2005; *Lunetta et al.*, 2005; *Dietz and Clausen*, 2008]. Since BiSN modeled watershed $NO_3^-$ export during a dry period and nonvegetation occurred at a low density in the West Fork watershed, one might expect the nonvegetation parameter not to be a major driver of watershed $NO_3^-$ export.

### 3.5. Big Sky Nutrient Export Model (BiSN)

[27] The relationship between LULC, watershed characteristics, and $NO_3^-$ export was determined by BiSN, whose modeling framework was adapted from the hybrid mechanistic N export coefficient approaches used by *Worrall and Burt* [1999], *Endreny and Wood* [2003], and *Johnes and Heathwaite* [1997]. Specifically, BiSN refined the basic export coefficient model by adding (1) a soil loss component, TSR, applicable watershed-wide but varying upon on geology (section 3.2) [modification from *Worrall and Burt*, 1999], (2) upland retention as a function of transport time from N source areas to the stream (TT) (section 3.41) [modification from *Endreny and Wood*, 2003 and *Johnes and Heathwaite*, 2003], (3) riparian buffering as a function of riparian to hillslope ratio (RBI) (section 3.4.1), (4) instream processing of N from upstream to downstream sites (decay) (section 3.1), (5) a Bayesian framework to assess the full range of predictive uncertainty (section 3.6), and (6) relatively dense spatial observations (section 3.1), which allowed for assessment of the relative role of terrestrial, riparian, and instream removal and how it varies along the stream network. The relevance of these additions to BiSN is discussed in the corresponding sections noted in parentheses.

[28] BiSN (equation (1a)) is broken into its components in equations (1b)–(1f), while a conceptual model is depicted in Figure 3B:

$$NE_i = \left[\sum_{j=1}^{n} \left(UL_j * URR_J\right)\right] - RR_i - IR_i, \tag{1a}$$

$$UL_j = VEG_j * b_{\mathrm{wg}} + WW_j * b_{\mathrm{ww}} + S_j * b_s + TSR_j * b_{\mathrm{tsr}} + WD_j * b_{\mathrm{wd}} + DD_j, \tag{1b}$$

$$URR_j = \frac{b_\beta}{TT_j^{(b_\beta - 1)}}, \tag{1c}$$

$$UR_i = \sum_{j=1}^{n} UL_j - \sum_{j=1}^{n} UL_j * URR_j, \tag{1d}$$

$$RR_i = RBI_i * b_i, \tag{1e}$$

$$IR_i = 0.5 * \mathrm{decay} + \left(NE_{\mathrm{up}} - \mathrm{decay}\right), \tag{1f}$$

where $NO_3^-$ export ($NE_i$ in kg d$^{-1}$) to the downstream end of stream reach $i$ (i.e., the size of the BiSN modeling unit) is modeled as a summation of (equation (1a)): (1) lateral $NO_3^-$ loading from the uplands ($UL_j$) decayed along terrestrial flow paths through the uplands ($URR_j$), the riparian zone ($RR_i$), and half of stream reach $i$ ($IR_i$), and (2) $NO_3^-$ loading from one or more adjacent upstream reaches decayed along the length of stream reach $i$ ($IR_i$).

[29] N loading to each upland pixel $j$ ($UL_j$) (equation (1b)) is the product of an indicator variable representing the existence of vegetation (*VEG*) or wastewater application (*WW*), the number of septic systems (*S*), terrestrial storage release of $NO_3^-$ (*TSR*), or wet deposition (*WD*) and the corresponding calibrated N export coefficient ($b_{\mathrm{veg}}$, $b_{\mathrm{ww}}$, $b_s$, $b_{\mathrm{tsr}}$, or $b_{\mathrm{wd}}$). Dry deposition (*DD*), was assumed constant across the watershed. Upland loading was considered in terms of total N because the speciation was not available or defensibly estimated for all loading sources. BiSN did not assume all N loading inputs were necessarily converted to nitrate, but it only attempted to model nitrate export.

[30] Terrestrial retention in BiSN occurs in the uplands ($UR_i$) and the riparian area ($RR_i$) of each reach contributing area and is a function of two terrain indices, watershed travel time (*TT*) and riparian buffering index (*RBI*). The N load from each upland pixel ($UL_j$) is modeled to follow a power law decay as it travels along hydrological flow paths to the stream as a function of $TT_j$ (equation (1c)). $UR_i$ is computed as the summation of $UL_j$ minus the summation of $UL_j$ decayed by $TT_j$ (equation (1d)). $NO_3^-$ exported from the uplands is subject to $RR_i$ (equation (1e)). $b_\alpha$ and $b_\beta$ are the calibrated shape and scale parameters of the power law function associated with $TT_j$, and $b_r$ is the calibrated *RBI* parameter.

[31] N loading that is exported from the riparian area is subject to instream retention ($IR_i$) (equation (1f)), which is a function of *decay* (areal retention, kg $d^{-1}$ $m^2$) inferred from instream $NO_3^-$ experiments conducted in the West Fork watershed during the study period (section 3.1 and Appendix A2). The other component of $IR_i$ is $NO_3^-$ exported from one or more upstream reach(es) ($NE_{up}$) (Figure 3B).

[32] $NO_3^-$ export was computed for each of the 231 stream reaches ($i = 231$) and compared to the observed $NO_3^-$ export at 50 stream reaches ($m = 50$). The total $NO_3^-$ export from the West Fork watershed is *NE* calculated at the most downstream reach (catchment outlet) and represents the integrated watershed response.

[33] Traditionally, N export coefficient methods have been applied to model the integrated watershed response at the catchment outlet without the ability to examine the internal spatial variability of processes controlling N export within the catchment. With the availability of dense spatial observations within the West Fork watershed, a major advantage of BiSN over other N export coefficient models is the ability to assess the spatial patterns in N export, N loading, and relative roles of N retention along the stream network from the headwaters to the catchment outlet.

### 3.6. BiSN Model Specification and Parameter Estimation

#### 3.6.1. BiSN Inference and Markov Chain Monte Carlo Methods

[34] Bayesian methods allow for "expert knowledge" of system behavior to be incorporated with observed data into model structure through the Bayes rule [*Gelman et al.*, 2004]:

$$P(\theta|NE) = \frac{P(\theta) * P(NE|\theta)}{P(NE)}, \quad (2)$$

where $P(\theta|NE)$ is the posterior distribution or the probability of the unknown model parameters $\theta$ given the observed data (*NE*), $P(\theta)$ is the prior distribution or the current knowledge of the model parameters, $P(NE|\theta)$ is the likelihood or the probability of the observed data given the parameters values, and $P(NE)$ is the prior probability of the observed data which acts as a normalizing constant. Emphasis is put on the posterior distribution of model parameters, which can provide a detailed description of parameter uncertainty leading to better quantification of model error and information for model diagnostics. Recent research in hydrologic modeling has shown Bayesian statistical inference to provide a powerful framework for assessing parameter uncertainty and subsequent uncertainty in applications such as rainfall-runoff model simulations [*Bates and Campbell*, 2001; *Marshall et al.*, 2004], groundwater flow [*Hassan et al.*, 2009], and solute export [*Qian*, 2005; *Zobrist and Reichert*, 2006; *Shrestha*, 2008]. This is because uncertainty in the model parameters can easily be assessed through the posterior distribution. Rather than a deterministic "best" single fit to the data, Bayesian methods estimate a distribution of possible parameter values. The Bayesian approach provides an attractive framework for inference in nutrient export modeling. This is especially true given the uncertainties in the export model parameters and processes, and the comparative lack of available data with which to constrain model results.

[35] Computation of the posterior distribution $P(\theta|NE)$ for most nonlinear models and models with a high dimensional parameter space can be prohibitively difficult [*Gelman et al.*, 2004]. For these cases, $P(\theta|NE)$ can be generated using a sampling algorithm. MCMC simulation methods are commonly used in Bayesian inference to estimate the posterior distribution by generating a sample from a distribution. BiSN was fit using an adaptive MCMC method for estimation of model parameters. The adaptive Metropolis algorithm (AM) [*Haario*, 2001] is a modification of the standard Metropolis algorithm, and has been shown to be advantageous for hydrologic modeling [*Marshall et al.*, 2004; *Hassan et al.*, 2009]. A major advantage of the AM algorithm is that the entire parameter set is updated simultaneously instead of each parameter individually, which reduces model complexity and thus, computational time.

[36] Following other hydrologic studies such as *Bates and Campbell* [2001], *Marshall et al.* [2004], *Zobrist and Reichert* [2006], *Hassan et al.* [2009], and *Smith and Marshall* [2010], the likelihood function assumed homoscedastic, uncorrelated error terms:

$$P(NE|\theta) = (2\pi\sigma^{-m/2}) \prod_m \left\{ -\frac{[NE_m - NE_i]^2}{2\sigma^2} \right\}, \quad (3)$$

where $\sigma^2$ is the error variance, $NE_m$ is observed nitrate export at stream reach $m$, and $NE_i$ is the corresponding modeled nitrate export obtained via Equation (1a).

#### 3.6.2. BiSN Implementation

##### 3.6.2.1. Prior Distributions

[37] The prior probability distribution represents the modeler's knowledge of system behavior. Prior knowledge of $b_{veg}$, $b_s$, and $b_r$ was based on literature values (Table 1) [*Rast and Lee*, 1984; *Burt et al.*, 1999; *McFarland et al.*, 2001; *US EPA*, 2002; *Maitre et al.*, 2003; *Zobrist and Reichert*, 2006; *Alexander et al.*, 2008; *NADP*, 2010]. Recognizing that literature values were based on studies conducted in watersheds with varying climatic and physical characteristics, prior bounds were loosely constrained by literature values. In general, prior bounds were within a order of magnitude of given literature values.

[38] The $b_{tsr}$, $b_{ww}$, and $b_{wd}$ parameters were constrained by empirical data collected in the study area (Table 1). $b_{ww}$ was constrained by unpublished wastewater N concentration and discharge data acquired from the Big Sky Water and Sewer District. Laboratory rock weathering experiments loosely bound the $b_{tsr}$ (Ackerman-Montross et al., manuscript in preparation, 2011). Inorganic N concentration data from Yellowstone National Park loosely constrained $b_{wd}$.

**Table 1.** Prior Distributions of BiSN Parameters and Corresponding References Used to Determine the Range of Possible Prior Values

| Variable | Calibrated Parameter | Prior Distribution | Prior Distribution Parameters | Units | Reference |
|---|---|---|---|---|---|
| Vegetation (*VEG*) | $b_v$ | uniform | $a = -3.65$ $b = 3.65$ | kg ha$^{-1}$ yr$^{-1}$ | *Alexander et al.*, 2008<br>*McFarland et al.*, 2001<br>*Rast and Lee*, 1983<br>*Zobrist and Reichert*, 2006 |
| Wastewater (*WW*) | $b_w$ | uniform | $a = 0$, $b = 3650$ | kg ha$^{-1}$ yr$^{-1}$ | Big Sky Water and Sewer District unpublished data |
| Septic (*S*) | $b_s$ | trapezoidal | $a = 0$, $b = 365$<br>$c = 1825$, $d = 2190$ | kg ha$^{-1}$ yr$^{-1}$ | *USEPA*, 2002 |
| Soil storage release (*TSR*) | $b_{\text{tsr}}$ | uniform | [0, 3650] | kg ha$^{-1}$ yr$^{-1}$ | Ackerman-Montross et al., manuscript in preparation, 2011 |
| Travel $\alpha$($TT_\alpha$) | $b_\alpha$ | uniform | [0, 1] | na | na |
| Travel $\beta$($\text{TT}_\beta$) | $b_\beta$ | uniform | [0, 1] | na | na |
| Wet depositon (*WD*) | $b_{\text{wd}}$ | trapezoidal | $a = 0.34$, $b = 0.55$<br>$c = 1.1$, $d = 1.36$ | mg L$^{-1}$ | *NADP*, 2010 |
| Riparian buffer (*RBI*) | $b_r$ | triangular | $a = -36.5$, $b = 182.5$<br>$c = 36.5$ | kg yr$^{-1}$ | *Burt et al.*, 1999<br>*Maitre et al.*, 2003 |

For the travel time parameters, the power law scale parameter, $b_\beta$, and the shape parameter, $b_\alpha$, were constrained between 0 and 1. During initial model runs, $b_\beta$ was unstable, so the parameter was fixed at its most probable value 0.035 based on initial model runs [*Bates and Campbell*, 2001].

[39] Expert knowledge informed the shape of each parameter's prior probability distributions (Table 1, Figure 7). Uninformative uniform prior probability distributions were applied for $b_\alpha$, $b_{\text{tsr}}$, $b_{\text{ww}}$, and $b_{\text{veg}}$. The uniform distribution applies equal probability to all values between the prior bounds. The $b_s$ and $b_{\text{wd}}$ parameters priors were assumed to be a generalized trapezoid distribution [*Seibert and McDonnell*, 2002], while the $b_r$ was assumed to be a triangular distribution [*Hession and Storm*, 2000].

#### 3.6.2.2. Model Convergence

[40] To ensure that the simulated posterior distribution was representative of the true posterior distribution, chain convergence was assessed by the Gelman-Rubin convergence diagnostic test [*Gelman and Rubin*, 1992]. The Gelman-Rubin diagnostic test is based on running multiple chains with starting points widely dispersed throughout the posterior distribution. The Gelman-Rubin approach diagnoses convergence by calculating the estimated potential scale reduction ($R$), which compares the variance within and between the multiple chains. At convergence $R$ should be close to 1.

[41] Model simulations were performed in Matlab. Each model simulation was run for 200,000 iterations. Pretuning runs were used to determine parameter values of high posterior probability to help initialize MCMC runs. Based on these runs, multiple chains with starting values chosen across the simulated posterior distribution were used to compute the Gelman-Rubin statistic and diagnose convergence to the posterior distribution.

#### 3.6.2.3. Predictive Uncertainty

[42] Total predictive uncertainty included uncertainties in the parameter values and the residual variance of the model output. We estimated total predictive uncertainty in our model simulations via MCMC parameter samples incorporating the effect of the model residual term.

## 4. Results

[43] Extrapolated to a yearly rate, observed stream water $NO_3^-$ export ranged from 0.0002 to 0.24 kg ha$^{-1}$ yr$^{-1}$. In the headwaters of the Middle Fork (Figure 1), streams draining Lone Mountain exported the highest amounts of stream water $NO_3^-$ (Figure 4). Lone Mountain is an alpine environment above tree line with steep slopes, consisting mainly of talus and scree. Inorganic N entering this environment with shallow soils, steep talus/scree slopes, and little riparian area could easily be transported through the system. Unfortunately, no data exists in the headwaters of the South Fork due to inaccessibility of private land. In addition, watershed $NO_3^-$ export was elevated in the lower reaches of the South Fork and the West Fork compared to other reaches. Both of these streams are alluvial streams draining areas of significant human development in the lower elevations of the watershed.

[44] Although we modeled stream water $NO_3^-$ in kg ha$^{-1}$ d$^{-1}$, we chose to report export values on an annual basis so that comparisons could easily be made with export values in the literature. We emphasize that reporting yearly $NO_3^-$ export based on summer $NO_3^-$ export underestimates yearly $NO_3^-$ export since the West Fork data was collected during summer low flow when $NO_3^-$ export is small compared to $NO_3^-$ export during the winter and snowmelt (Gardner and McGlynn, manuscript in preparation, 2011).

### 4.1. Model Performance and Predictive Uncertainty

[45] The calibration of BiSN converged after 100,000 iterations (the Gelman Rubin diagnostic $R \sim 1$) for all parameters; therefore, the subsequent results are based on iterations 100,001 to 200,000. Modeled versus observed stream water $NO_3^-$ export with 90% prediction intervals are illustrated in Figure 5. Overall, the spatial variability of observed stream water $NO_3^-$ export was well captured by BiSN over a wide range of environmental and land use gradients (Figures 5 and 6); the Nash-Sutcliffe model efficiency coefficient was 0.90 (Figure 6). Model residuals were normally distributed, and did not appear to be homoscedastic (Figure 6) or spatially correlated. Since 93% of the observed data fell between the 90% prediction intervals (Figure 5) and there was no pattern in the model residuals, we can assume that the likelihood assumptions were appropriate.

### 4.2. Parameter Estimates

[46] The parameter distributions produced by the MCMC sampling algorithm are illustrated in Figure 7. There was no

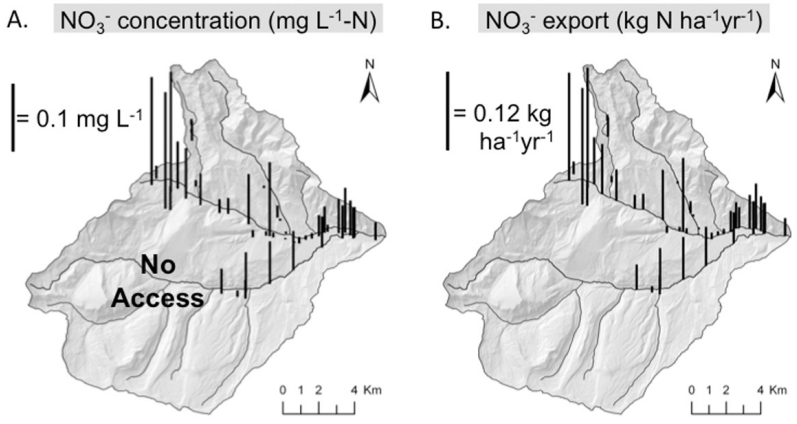


**Figure 4.** (A) Observed spatial $NO_3^-$ concentrations (black bars) from 7 August 2007. $NO_3^-$ concentration is greatest in the headwaters of the Middle Fork and elevated in the South Fork and West Fork compared to other streams. (B) When N export is normalized for watershed area, $NO_3^-$ export pattern mirrors the patterns of concentrations; $NO_3^-$ export is greatest in the headwaters of the Middle Fork and elevated in the South Fork and West Fork compared to other streams. Height of the black bars corresponds to $NO_3^-$ export values. There is no data from the headwaters of the South Fork because landowner refused access.

significant correlation among any parameters. Parameters for the BiSN model parameters varied in their identifiability, which refers to the ability of a model and data to constrain a parameter [*Luo et al.*, 2009]. $b_{ww}$ (Figure 7B) and $b_\alpha$ (Figure 7E) were most identifiable; a clear peak was evident in their posterior distributions. $b_{ww}$ was most likely about 10 kg $ha^{-1}$ $yr^{-1}$, while $b_\alpha$ was most likely between 0.4 and 0.7. $b_{tsr}$ (Figure 7D) and $b_r$ (Figure 7G) had regions of their parameter space that were more likely than others. $b_{tsr}$ was most likely at the lower end of the prior distribution, between 100 and 500 kg $ha^{-1}$ $yr^{-1}$ (Figure 7D) for grid cells with geology more prone to weather N; however, most of the watershed consisted of geology less prone to weather N, which corresponded to $b_{tsr}$ values between 10 and 50 kg $ha^{-1}$ $yr^{-1}$. Riparian buffer $b_r$ was most likely greater than zero, indicating increasing N retention with increasing riparian to hillslope ratios (equations (1)).

[47] The posterior distributions of $b_{veg}$ (Figure 7A), $b_s$ (Figure 7C), and $b_{wd}$ (Figure 7F) were less identifiable than other parameters as illustrated by relatively flat posterior distributions. Even though stream water $NO_3^-$ export was less sensitive to N inputs from vegetation, septic, or wet deposition, a few general observations that could be made

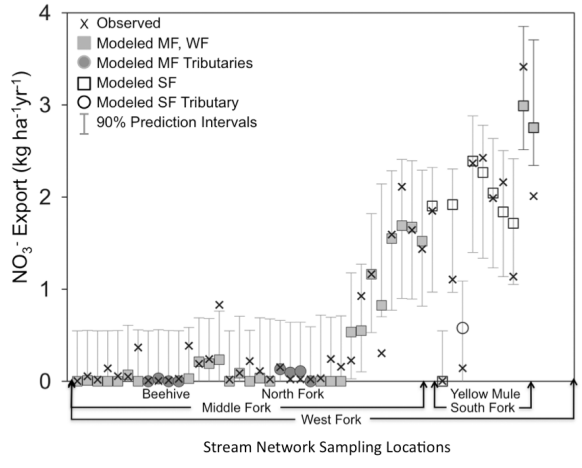


**Figure 5.** The spatial variability of observed stream water $NO_3^-$ export (black x's) was well captured by BiSN over a wide range of land use/land cover and landscape positions with 90% prediction intervals (gray lines). 93% of observed data falls within the 90% prediction intervals. Data is ordered to depict network organization. The spatial variability of observed stream water $NO_3^-$N export (black x's) was well captured by BiSN over a wide range of land use/land cover and landscape positions with 90% prediction intervals (gray lines). 93% of observed data falls within the 90% prediction intervals. Data is ordered to depict network organization. From the headwaters, the Middle Fork flows into the West Fork (gray squares). Tributaries to the Middle Fork include Beehive and the North Fork (gray circles), to the West Fork include the South Fork, and to the South Fork include Yellow Mule (black outlined circle).

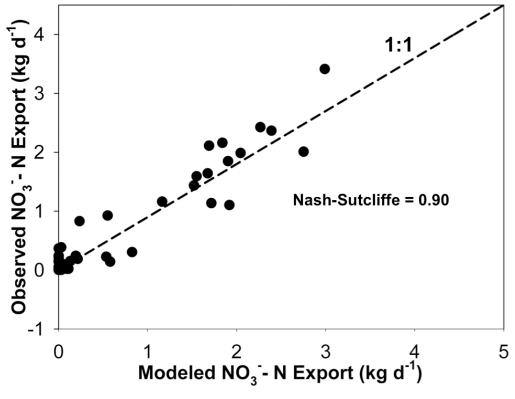


**Figure 6.** BiSN was a good predictor of stream water $NO_3^-$ export (Nash-Sutcliffe model efficiency coefficient = 0.90). Model residuals were normally distributed and did not appear to have a pattern about the 1:1 line or to be spatially correlated.

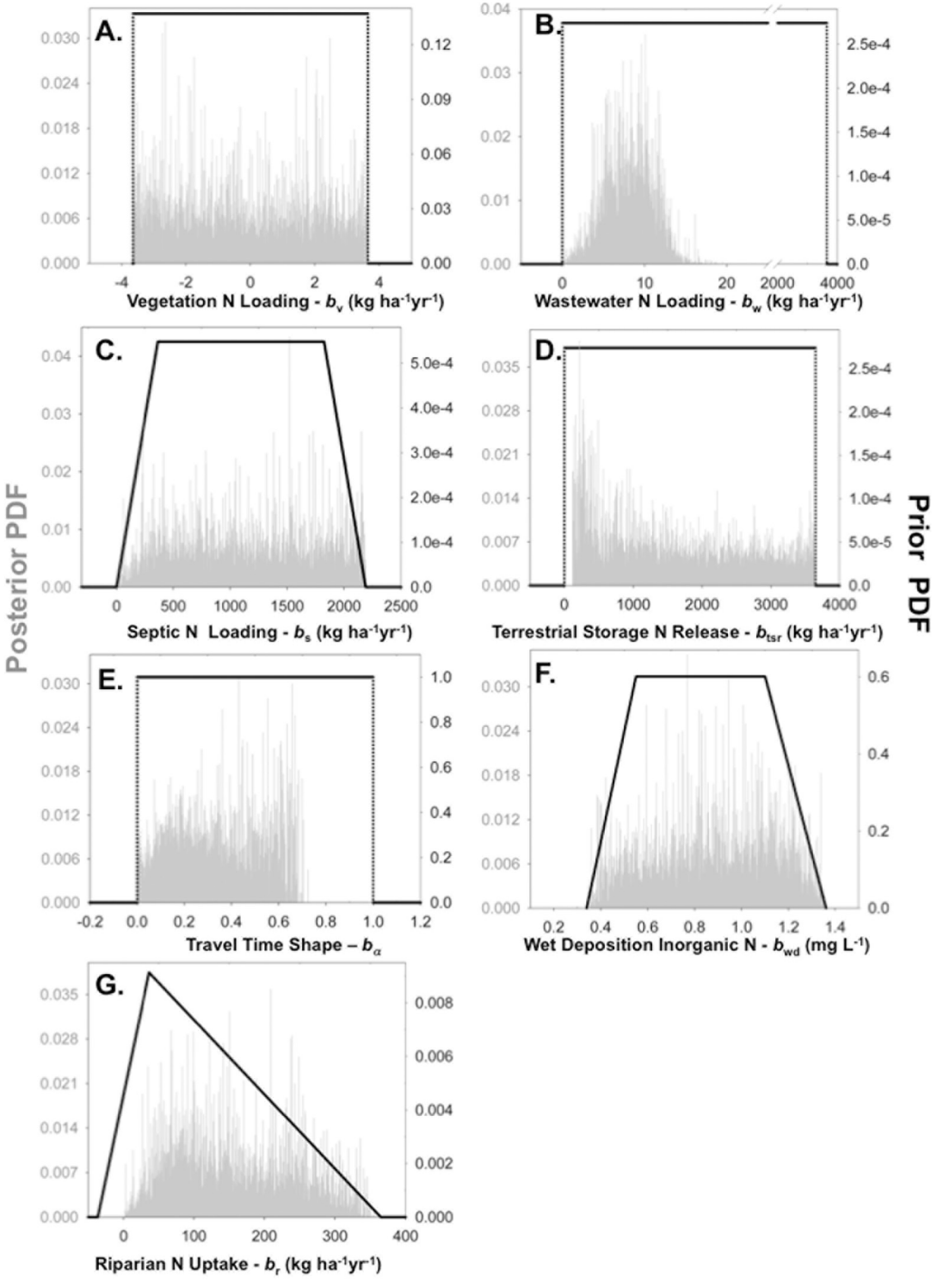


**Figure 7.** (A–G) Histograms of model posterior distributions (gray) with corresponding prior distributions (black). Parameters vary in their identifiability: the wastewater (B) and travel parameters (G) were most identifiable, while the vegetation (A) and septic (C) parameters were least identifiable.

about their posterior distributions: (1) $b_{veg}$ was most likely an N sink, (2) $b_s$ had the highest probability of being near 1500 kg ha$^{-1}$ yr$^{-1}$, and (3) $b_{wd}$ was most likely between 0.7 and 1.1 mg L$^{-1}$. Although some posterior distributions do appear bimodal ($b_{veg}$, $b_s$, and $b_{tsr}$), there was no significant relationship between any two variables.

[48] The parameter values that produced the maximum likelihood and minimum variance are presented with their 90% confidence intervals in Table 2. These values were applied to assess BiSN's capability to estimate observed stream water $NO_3^-$ export (Figure 4A) and to calculate N loading, retention, and export by reach contributing area.

**Table 2.** Parameter Values Corresponding to the Maximum Log-Likelihood of BiSN Runs[a]

| Parameter | Maximum Likelihood | Units |
|---|---|---|
| *VEG* | 2.734 | kg ha$^{-1}$ yr$^{-1}$ |
| *WW* | 10.439 | kg ha$^{-1}$ yr$^{-1}$ |
| *S* | 336.530 | kg ha$^{-1}$ yr$^{-1}$ |
| *TSR* | 297.402 | kg ha$^{-1}$ yr$^{-1}$ |
| $TT_a$ | 0.619 | na |
| $TT_b$ | 0.035 | na |
| *WD* | 1.150 | mg L$^{-1}$ |
| *RBI* | 270.427 | kg ha$^{-1}$ yr$^{-1}$ |

[a]Abbreviations for parameters are described in Table 1.

The maximum likelihood parameter estimates of N loading from $b_s$ and $b_{tsr}$ were highest at 336.5 and 297 kg ha$^{-1}$ yr$^{-1}$, respectively. $b_{tsr}$ of 297 kg ha$^{-1}$ yr$^{-1}$ corresponded to terrestrial storage release of $NO_3^-$ from areas consisting of geology with high potential to weather $NO_3^-$, while terrestrial storage release of $NO_3^-$ from areas with low potential to weather $NO_3^-$ corresponded to a $b_{tsr}$ value of 29.7 kg ha$^{-1}$ yr$^{-1}$. Although their export parameter values were similar, N loading from septic systems and terrestrial storage release is quite different and has ramifications for stream water $NO_3^-$ export. Septic systems export effluent to a localized area, but the actual loading value appears smaller because it is normalized across a hectare. Localized highly concentrated septic loading has potential to saturate the immediate disposal area and be quickly transported to streams. On the other hand, inorganic N released from terrestrial storage is evenly dispersed across a hectare and can provide more opportunity for plant and microbial immobilization of $NO_3^-$ leading to less $NO_3^-$ transported to streams.

[49] Vegetated land exported the least amount of N at 2.73 kg ha$^{-1}$ yr$^{-1}$ (Table 2); however, based on the 90% confidence intervals, $b_{veg}$ could have been a net sink or source of N. The maximum likelihood estimate for $b_{wd}$ was 1.15 mg L$^{-1}$, with an upper and lower 90% confidence limit of 0.5 and 1.34 mg L$^{-1}$. $b_r$ was estimated as a net sink of $NO_3^-$, removing 270 kg ha$^{-1}$ yr$^{-1}$, which was toward the upper end of the prediction interval (40 to 286 kg ha$^{-1}$ yr$^{-1}$). $b_\alpha$ was estimated to be 0.619, while was fixed at 0.035.

### 4.3. Drivers of the Spatial Heterogeneity of Stream Water $NO_3^-$ Export

[50] The spatial network structure of BiSN allows for exploration of N loading (equation (1b)), export and retention (equations (1d)–(1f)) patterns at the watershed scale. Source $NO_3^-$ contributions for each reach contributing area was calculated by multiplying the maximum likelihood parameter estimates by the N source areas and then dividing by the total reach contributing area (Table 3). Total N loading is presented in Figures 8A and 8C and Table 3, while $NO_3^-$ exported from the uplands (i.e., N loading decayed by relative travel time) is presented in Figures 8B and 8D and Table 3. Terrestrial storage release of $NO_3^-$ dominated N loading across the watershed (Figure 8A). Excluding terrestrial storage release of $NO_3^-$ to illuminate other source contributions, the relative N loading across the watershed was very similar with the exception of a high septic load in the upper Middle Fork (MFHW1) (Figure 8C). Very little $NO_3^-$ was exported from the uplands except for in the main stem West Fork, where wastewater contributions to $NO_3^-$ export were high (Figure 8D, Table 4). Although the wastewater load was relatively small compared to other sources, it had a disproportionately large contribution to upland $NO_3^-$ export (Figure 8D).

[51] The relative contributions of the three watershed N retention components (upland, riparian, and instream) are depicted in Figure 9 and Table 4. The majority of $NO_3^-$ (98–99%) was retained in the uplands (Figure 9A, Table 4).

**Table 3.** Modeled Sources of N Loading for Subwatersheds Corresponding to Figures 8 and 9[a]

| Map Code | Subwatershed | Area (ha) | *VEG* (kg ha$^{-1}$ yr$^{-1}$) | *WW* (kg ha$^{-1}$ yr$^{-1}$) | *S* (kg ha$^{-1}$ yr$^{-1}$) | *TSR* (kg ha$^{-1}$ yr$^{-1}$) | *WD* (kg ha$^{-1}$ yr$^{-1}$) | *DD* (kg ha$^{-1}$ yr$^{-1}$) | Total N Inputs (kg ha$^{-1}$ yr$^{-1}$) |
|---|---|---|---|---|---|---|---|---|---|
| 1 | Upper Beehive (UB) | 299 | 1.79 | 0 | 0 | 30.22 | 3.18 | 0.26 | 35.46 |
| 2 | Beehive (BH) | 833 | 2.28 | 0.00 | 0.71 | 44.90 | 2.94 | 0.26 | 51.09 |
| 3 | MF Headwaters 1 (MFHW1) | 88 | 1.91 | 0.00 | 9.36 | 29.97 | 2.86 | 0.26 | 44.37 |
| 4 | MF Headwaters 2 (MFHW2) | 380 | 2.51 | 0.00 | 0.39 | 33.11 | 2.81 | 0.26 | 39.08 |
| 5 | Upper Middle Fork (UMF) | 1280 | 2.09 | 0.00 | 2.44 | 31.31 | 2.80 | 0.26 | 38.89 |
| 6 | Middle Middle Fork (MMF1) | 2773 | 2.16 | 0.00 | 1.45 | 44.02 | 2.78 | 0.26 | 50.67 |
| 7 | Middle Middle Fork (MMF2) | 4786 | 2.27 | 0.00 | 1.74 | 37.93 | 2.66 | 0.26 | 44.87 |
| 8 | Upper North Fork (UNF) | 378 | 1.65 | 0.00 | 0.00 | 29.87 | 3.14 | 0.26 | 34.92 |
| 9 | Middle North Fork (MNF) | 1077 | 2.02 | 0.00 | 0.00 | 37.49 | 3.00 | 0.26 | 42.77 |
| 10 | Lower North Fork (LNF) | 2319 | 2.23 | 0.00 | 0.23 | 35.58 | 2.90 | 0.26 | 41.20 |
| 11 | UpperWest Fork (LMF) | 8412 | 2.24 | 0.20 | 1.27 | 38.84 | 2.69 | 0.26 | 45.49 |
| 12 | South Fork Headwaters (SFH) | 1898 | 2.15 | 0.00 | 0.02 | 29.86 | 2.98 | 0.26 | 35.27 |
| 13 | Upper South Fork (USF) | 2565 | 2.12 | 0.00 | 0.33 | 41.38 | 2.93 | 0.26 | 47.02 |
| 14 | Upper Muddy Creek (UMC) | 1913 | 2.17 | 0.00 | 0.00 | 49.91 | 3.00 | 0.26 | 55.34 |
| 15 | Third Yellow Mule (3YM) | 633 | 2.24 | 0.00 | 0.00 | 124.52 | 3.02 | 0.26 | 130.04 |
| 16 | Lower Muddy Creek (LMC) | 3577 | 2.19 | 0.00 | 0.03 | 59.08 | 2.94 | 0.26 | 64.50 |
| 17 | Second Yellow Mule (2YM) | 1148 | 2.46 | 0.00 | 0.00 | 160.53 | 2.90 | 0.26 | 166.15 |
| 18 | Middle South Fork1 (MSF1) | 8020 | 2.20 | 0.00 | 0.20 | 66.53 | 2.88 | 0.26 | 72.07 |
| 19 | Upper Yellow Mule (UYM) | 464 | 2.26 | 0.00 | 0.00 | 186.03 | 2.97 | 0.26 | 191.52 |
| 20 | Lower Yellow Mule (LYM) | 1101 | 2.51 | 0.00 | 0.00 | 115.04 | 2.81 | 0.26 | 120.62 |
| 21 | Middle South Fork2 (MSF2) | 11,068 | 2.27 | 0.00 | 0.16 | 68.71 | 2.82 | 0.26 | 74.23 |
| 22 | Lower South Fork (LSF) | 11,971 | 2.29 | 0.00 | 0.38 | 66.00 | 2.77 | 0.26 | 71.71 |
| 23 | Lower West Fork (WF) | 20,617 | 2.27 | 0.09 | 0.77 | 54.41 | 2.73 | 0.26 | 60.52 |

[a]Map codes correspond to sites depicted in Figure 9A. Abbreviations for column headings described in Table 1.

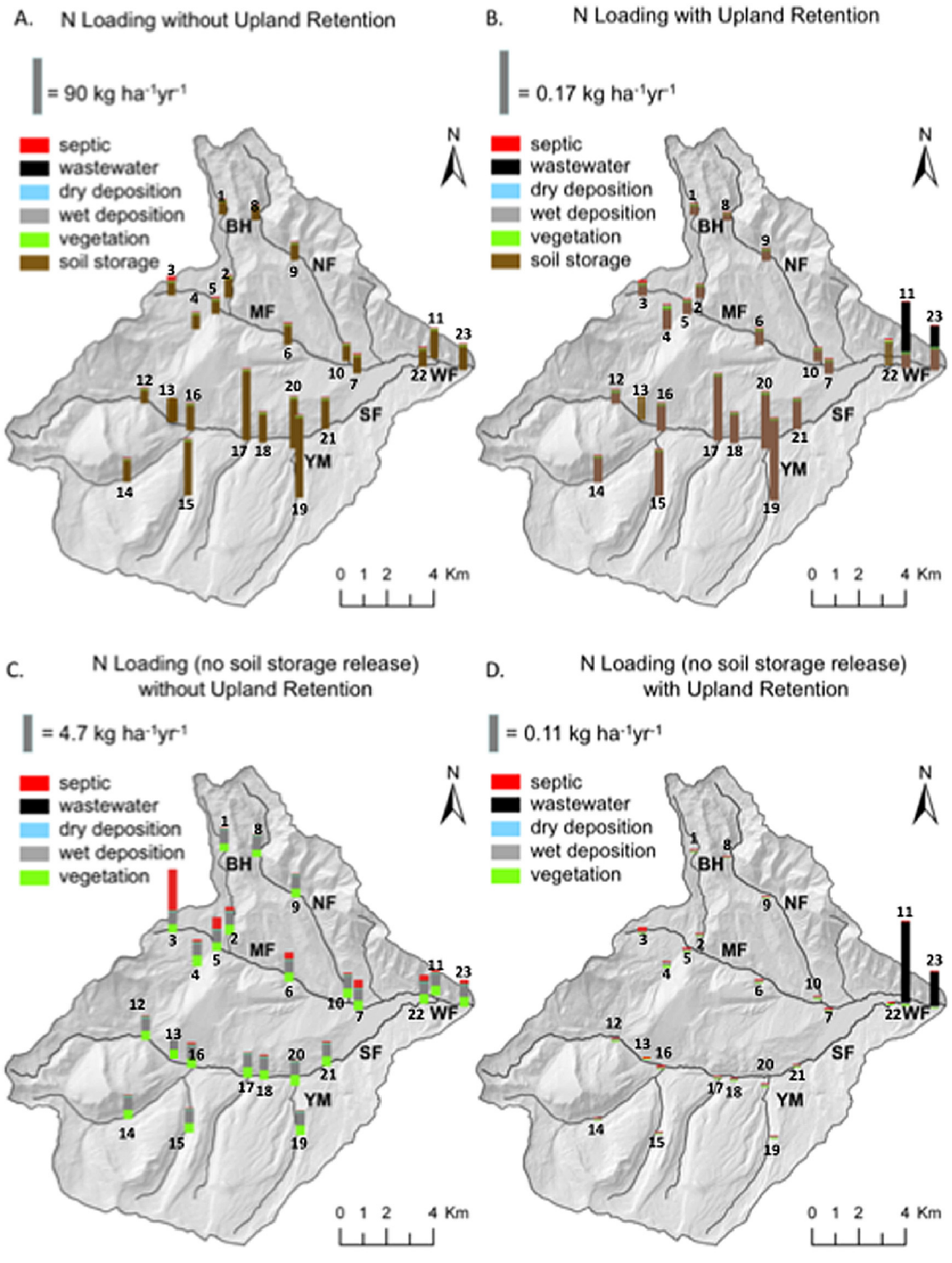


**Figure 8.** Modeled N loading across the West Fork watershed (A) compared to N loading after travel time decay is applied (B). N originating from soil storage release dominated the $NO_3^-$ signal. Excluding N loading from soil storage release (C, D), localized small inputs of anthropogenic N from wastewater were responsible for elevated stream water $NO_3^-$ export in the lower section of the West Fork (D). Wastewater inputs, which occurred "hydrologically close" to the stream and were smaller relative to other N inputs, had a disproportionate impact on watershed $NO_3^-$ export.

**Table 4.** Relative Importance of Upland, Riparian, and Instream N Retention for Subwatersheds Listed in Table 3[a]

| Map code | Subwatershed | Total N Inputs (kg ha$^{-1}$ yr$^{-1}$) | Upland N Retention (kg ha$^{-1}$ yr$^{-1}$) | Riparian N Retention (kg ha$^{-1}$ yr$^{-1}$) | Instream N Retention (kg ha$^{-1}$ yr$^{-1}$) | $NO_3^-$–N Export (kg ha$^{-1}$ yr$^{-1}$) |
|---|---|---|---|---|---|---|
| 1 | Upper Beehive (UB) | 35.46 | 34.93 (99) | 0.26 (49) | 0.26 (50) | 0.003 (1) |
| 2 | Beehive (BH) | 51.09 | 50.72 (99) | 0.26 (71) | 0.10 (26) | 0.011 (3) |
| 3 | Middle Fork Headwaters 1 (MFHW1) | 44.37 | 44.02 (98) | 0.08 (23) | 0.05 (13) | 0.226 (64) |
| 4 | Middle Fork Headwaters 2 (MFHW2) | 39.08 | 38.80 (98) | 0.04 (16) | 0.19 (67) | 0.050 (17) |
| 5 | Upper Middle Fork (UMF) | 38.89 | 38.62 (99) | 0.15 (55) | 0.09 (34) | 0.030 (11) |
| 6 | Middle Middle Fork (MMF) | 50.67 | 50.36 (99) | 0.19 (60) | 0.124 (39) | 0.006 (1) |
| 7 | Lower Middle Fork (MF) | 44.87 | 44.46 (99) | 0.18 (44) | 0.23 (55) | 0.001 (1) |
| 8 | Upper North Fork (UNF) | 34.92 | 34.77 (99) | 0.09 (62) | 0.05 (33) | 0.006 (4) |
| 9 | Middle North Fork (UNF) | 42.77 | 42.59 (99) | 0.094 (52) | 0.085 (47) | 0.0002 (<1) |
| 10 | Lower North Fork (LNF) | 41.20 | 40.89 (99) | 0.13 (43) | 0.17 (56) | 0.003 (2) |
| 11 | Upper West Fork (UWF) | 45.49 | 44.78 (98) | 0.21 (29) | 0.44 (63) | 0.059 (11) |
| 12 | South Fork Headwaters (SFH) | 35.27 | 35.11 (99) | 0.12 (72) | 0.045 (27) | 0.0002 (<1) |
| 13 | Upper South Fork (USF) | 47.02 | 46.79 (99) | 0.12 (49) | 0.12 (50) | 0.0003 (<1) |
| 14 | Upper Muddy Creek (UMC) | 55.34 | 54.89 (99) | 0.097 (22) | 0.35 (78) | 0.002 (1) |
| 15 | Third Yellow Mule (3YM) | 130.04 | 129.62 (99) | 0.12 (29) | 0.24 (57) | 0.05 (13) |
| 16 | Lower Muddy Creek (LMC) | 64.50 | 64.04 (99) | 0.11 (24) | 0.35 (76) | 0.0002 (<1) |
| 17 | Second Yellow Mule (2YM) | 166.15 | 164.56 (98) | 0.082 (5) | 1.45 (91) | 0.06 (4) |
| 18 | Middle South Fork1 (MSF1) | 72.07 | 71.26 (98) | 0.12 (15) | 0.65 (83) | 0.040 (2) |
| 19 | Upper Yellow Mule (UYM) | 191.52 | 189.82 (99) | 0.15 (9) | 1.40 (82) | 0.16 (9) |
| 20 | Lower Yellow Mule (LYM) | 120.62 | 119.55 (99) | 0.18 (17) | 0.88 (82) | 0.012 (1) |
| 21 | Middle South Fork2 (MSF2) | 74.23 | 73.15 (98) | 0.14 (13) | 0.87 (80) | 0.080 (7) |
| 22 | Lower South Fork (LSF) | 71.71 | 70.40 (98) | 0.15 (11) | 1.13 (86) | 0.035 (3) |
| 23 | Lower West Fork (WF) | 60.52 | 59.39 (98) | 0.18 (15) | 0.96 (82) | 0.035 (3) |

[a]Percent retention excluding upland retention is in parentheses. Map codes correspond to sites depicted in Figure 9A.

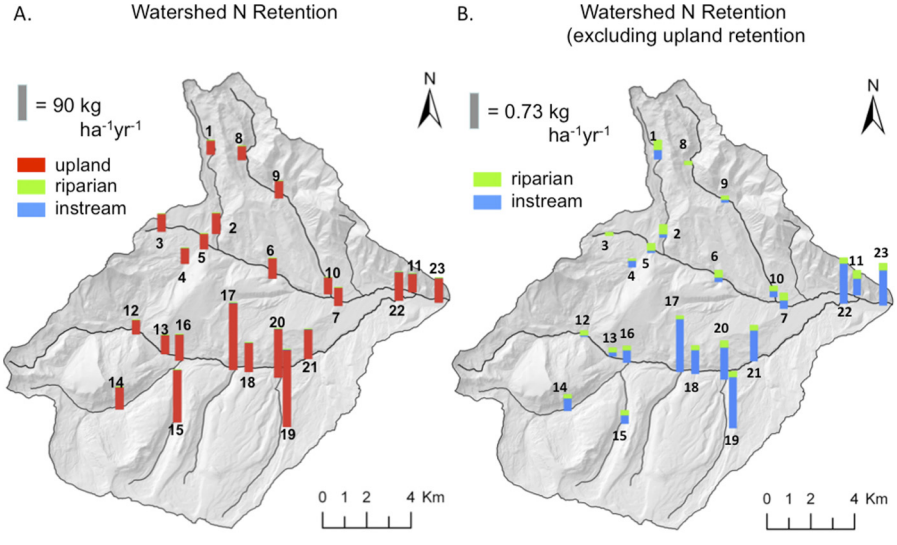


**Figure 9.** Modeled upland, instream, and riparian $NO_3^-$ retention across the West Fork watershed. (A) Most N loading was retained in the upland by either biological processes or lack of a physical transport mechanism (hydrological connectivity). (B) Excluding upland retention, instream processes were responsible for more $NO_3^-$ immobilization than riparian areas in the majority of the watershed. Numbers correspond to map codes in Tables 3 and 4.

Instream $NO_3^-$ retention was substantially greater than riparian $NO_3^-$ retention in the South Fork, the lower Middle Fork, and the West Fork (Figure 9B). In headwaters of the South Fork, the Middle Fork and the North Fork, there were differences in the relative amounts of riparian and instream $NO_3^-$ retention. In the headwaters of the South Fork watershed, instream processes generally immobilized more $NO_3^-$ than the riparian area. Conversely, in the Middle Fork and North Fork the riparian area generally immobilized more $NO_3^-$ than instream processes. In addition, the magnitude of riparian and instream retention was significantly higher in the South Fork than the Middle and North Forks.

## 5. Discussion

### 5.1. Model Performance and Predictive Uncertainty

[52] BiSN integrated stream chemistry from spatial sampling and $NO_3^-$ tracer additions with terrain and land use analysis in a Bayesian framework to estimate sources of watershed N loading, $NO_3^-$ export, and retention. As a relatively simple model with the goal of minimizing model parameters and predictive uncertainty, BiSN's minimal data requirements included: observed stream water $NO_3^-$ concentrations, a DEM, locations and approximate N loads of wastewater sources, and maps of land use/cover and geology.

[53] Although the prediction intervals, which include uncertainties in parameter values and model residuals, were fairly wide, they did capture the general patterns of stream water $NO_3^-$ export of streams ranging from pristine first-order streams draining high-elevation alpine-subalpine watersheds (Beehive) to a fourth-order alluvial bottom stream draining substantial human development (West Fork). Analysis of predictive uncertainty, which incorporated parameter uncertainty (Figure 6), is a major advancement in our analysis approach compared to other export coefficient modeling approaches. In BiSN, parameter uncertainty implied that the exact allocation of each $NO_3^-$ source/sink is unknown. The degree of uncertainty for each parameter was reflected in the full range and shape of the parameter posterior distributions.

[54] The majority of studies applying export coefficient models have judged model performance solely by stating some goodness of fit measure that compares observed and predicted observations (i.e., $R^2$, Nash-Sutcliffe, percent error, etc.) [*Worrall and Burt*, 1999, 2001; *Johnes*, 1996; *Whitehead et al.*, 2002]. Some studies have attempted to account for uncertainty in export coefficient parameters by surveying the full range of export coefficient values observed across multiple watersheds [*Reckhow et al.*, 1980; *Griffin*, 1995; *McFarland and Hauck*, 2001; *Wickham and Wade*, 2002; *Endreny and Wood*, 2003]; however, this representation reflects the variability in export coefficients not their uncertainty [*Khadam and Kaluarachchi*, 2006]. Other studies have recognized the high uncertainty inherent in export coefficients [*Zobrist and Reichert*, 2006; *Khadam and Kaluarachchi*, 2006]; however, these studies did not report how parameter uncertainty impacted model predictions of watershed nutrient export. Effects of parameter uncertainties on model performance can be substantial and should be evaluated to ensure the precision and reliability of the predicted results [*Beck*, 1987].

[55] Reliability of predicted results can also be affected by spatial correlation among model residuals [*Cressie*, 1993]. Recent research has shown spatial dependency to exist in water quality data [*Dent and Grimm*, 1999; *Peterson et al.*, 2006; *Gardner and McGlynn*, 2009]. Spatial processes governing $NO_3^-$ export were implicitly incorporated within the BiSN network structure: each reach had $NO_3^-$ inputs from upstream reaches and $NO_3^-$ outputs that influenced downstream reaches (Figure 3B). The absence of spatial correlation among model residuals suggests that the spatial relationship between upstream and downstream reaches was well characterized in BiSN.

### 5.2. Drivers of the Spatial Heterogeneity of Stream Water $NO_3^-$ Export

[56] BiSN's output provided insight into the main drivers of stream water $NO_3^-$ export in the West Fork watershed during the summer growing season. Specifically, the shape and range of the parameter posterior distributions reflect the relative influence of each parameter on stream water $NO_3^-$ export.

[57] Model parameters had a wide range of influence on modeled stream water $NO_3^-$ export (Figure 7), as demonstrated by their posterior distributions. Modeled stream water $NO_3^-$ export was most sensitive to $b_{ww}$ (Figure 7B) and $b_\alpha$ (Figure 7G). N loading from wastewater irrigation on the Big Sky Resort Golf Course, which drains into the upper West Fork, just before the confluence with the South Fork (Figure 1). Although the amount of N loading to the Big Sky Golf Course is relatively small (Figures 8A and 8C, Table 2), it had a disproportionately large impact on stream water $NO_3^-$ export (Figure 8B and 8D, Table 3). Golf course irrigation with treated wastewater occurs over a short time period (approximately May through October) onto an area with very short relative travel times to the stream. Consequently, there is limited potential for biological retention of $NO_3^-$ and the majority of N loading is readily transported through shallow groundwater to the upper West Fork.

[58] The other strongly identifiable parameter $b_\alpha$ (Figure 7E) describes the rate at which N loading is retained or removed as it moves through the landscape. N loading occurring "hydrologically close" to the stream (short relative travel times) has the potential for greater impact on stream water $NO_3^-$ than N loading occurring "hydrologically farther away" (longer relative travel times) because of increased time and distance for N retention. Other relatively simple N export models have also found improved model performance by adding parameters that describe hydrologic transport times [*Smith*, 1997; *Johnes and Heathwaite*, 1997; *Frateriggo and Downing*, 2008; *Gardner and McGlynn*, 2009].

[59] Although not as sensitive as $b_{ww}$ and $b_\alpha$, $b_{tsr}$ (Figure 7D) and $b_r$ (Figure 7G) did have regions of their modeled parameter space that were more likely than others. $b_{tsr}$ was most probable between 100 and 500 kg $ha^{-1}$ $yr^{-1}$ (Figure 7D); therefore, terrestrial storage in areas associated with mineralogy more prone to weather N exported between 100 and 500 kg $ha^{-1}$ $yr^{-1}$, while terrestrial storage in areas associated with mineralogy less prone to weather N exported 10 to 50 kg $ha^{-1}$ $yr^{-1}$. The high values of terrestrial storage release of N that occurred in 9% of the

watershed were justified by the laboratory weathering experiments (Ackerman-Montross et al., manuscript in preparation, 2011). Other work has estimated geologic sources to contribute significantly (90%) to stream water $NO_3^-$ concentrations [*Holloway*, 1998, 1999]. This high contribution of geologic N implies that future research should further investigate the relationships between ground and surface water chemistry and geologic N sources.

[60] Terrestrial storage can be a significant sink of watershed N and has been has been estimated to be anywhere from 2000 kg $ha^{-1}$ in warm deserts to 20,000 kg $ha^{-1}$ in wet tropical systems [*Post et al.*, 1985]. Two sources of terrestrial storage release, N fixation and mineralization, were not directly included as parameters in BiSN. Instead their contributions were lumped into $b_{tsr}$. Studies have shown that N fixation from terrestrial [*Fahey et al.*, 1985; *Cleveland et al.*, 1999; *Vitousek et al.*, 2002; *Jacot et al.*, 2009] and aquatic [*Meyer et al.*, 1981; *Grimm and Petrone*, 1997; *Triska*, 1984] ecosystems can be substantial sources of watershed N. In addition to N fixation, mineralization of organic matter can be a significant contributor to watershed N export [*Bormann*, 1977; *Fisk and Schmidt*, 1995; *Brooks et al.*, 1996; *Ross et al.*, 2009]. Mineralization is the release of inorganic N from the microbial break down of organic matter. Research has shown watershed net mineralization rates to be highly variable, from $<1$ to 37 kg $ha^{-1}$ $yr^{-1}$, which is in the range of terrestrial storage release from sites with low potential for geologic release of N. Mineralization rates can depend on soil temperature, soil moisture [*Hong et al.*, 2004; *Miller et al.*, 2009], soil C:N ratios [*Janssen*, 1996; *Springob and Kirchmann*, 2003], snowcover [*Brooks et al.*, 1996; *Miller et al.*, 2009], and vegetation and soil type [*Hart and Firestone*, 1991]. In addition to mineralization, soil disturbance from freeze thaw cycles can destroy fine roots and disturb microbiological communities decreasing N immobilization thereby releasing more inorganic N [*Groffman et al.*, 2001].

[61] *Worrall and Burt* [1999] introduced a soil reserve parameter representing the release of inorganic N from soil organic matter to the basic export coefficient model. The optimized soil reserve parameter, which was applied as a weighting function to plowed agricultural land, was 80 kg $ha^{-1}$ $yr^{-1}$, which falls in the range of $b_{tsr}$ values in areas with geology less prone to weather N. In the West Fork watershed, soil disturbance from land clearing associated with ski resort development could similarly disturb soils and be responsible for the high release of inorganic nitrogen from soils.

[62] Similar to $b_{tsr}$, $b_r$ illustrated a range of values that were more likely than others. $b_r$ was most likely greater than zero, meaning that watershed $NO_3^-$ retention and/or removal increased with increasing riparian to hillslope ratios (Figure 7G, equations (1)). As the interface between the terrestrial and aquatic ecosystems, riparian ecosystems can be hot spots for $NO_3^-$ immobilization. However the riparian buffer's ability to remove $NO_3^-$ can be highly variable depending on (1) the proximity of the water table to the root zone, (2) the groundwater flow rate, (3) the width of the riparian zone, (4) temperature, and (5) the labile carbon supply for microbial denitrification [*Burt et al.*, 1999; *Lowrance et al.*, 1984; *Hill*, 1996; *Maitre et al.*, 2003; *Dent et al.*, 2007]. Conversely, riparian areas can also be significant sources of organic N [*Schade et al.*, 2002]. At the watershed scale, many of these factors controlling storage and release of N in the riparian area are highly variable. Since BiSN generalized riparian control of N through the terrain index RBI and did not explicitly account for the variability of these factors, we might expect $NO_3^-$ retention occurring in the riparian buffers difficult to identify.

[63] The remaining model parameters ($b_s$, $b_{wd}$, and $b_{veg}$) had modeled posterior distributions that were less identifiable than other parameters. The posterior distribution of $b_s$ illustrated septic system N loading was most likely greater than 250 kg $ha^{-1}$ $yr^{-1}$ (Figure 7C). Variability in septic system N loading is expected due to the seasonality of second home use and the variability in the number of people using each system.

[64] Although septic effluent has high concentrations of inorganic N [*EPA*, 2002], septic systems contributed very little to upland $NO_3^-$ across the West Fork watershed (Figures 8B and 8D). There are two plausible explanations for their limited impact on upland $NO_3^-$ export: (1) septic systems are widely dispersed across the 212 $km^2$ West Fork watershed and the effluent is either diluted and/or readily immobilized before it reaches the stream or (2) the septic systems have a limited or nonexistent hydrological connectivity to the stream. Previous research showed distinct seasonality in the influence of septic systems on stream water $NO_3^-$ concentrations in the West Fork watershed [*Gardner and McGlynn*, 2009]. During the growing season, septic system effluent may be quickly immobilized along hydrological pathways before it reaches the stream network. Other research has shown increased septic system distance from surface water can decrease septic influence on surface water N [*Meile et al.*, 2010]; however, septic $NO_3^-$ removal can be limited if carbon is limiting microbial denitrification [*Colman et al.*, 2004]. It is possible that hydrologic connectivity between septic systems and the streams was limited or nonexistent preventing septic effluent transport to the stream.

[65] $b_{wd}$ was tightly constrained by observed data (Figure 7F), which could explain it is relatively flat posterior distribution. The posterior distribution suggested that $b_{wd}$ was most probable between 0.7 and 1.1 mg $L^{-1}$. The variability in $b_{wd}$ posterior values could result from (1) N at these low concentrations being readily retained and/or removed (biologically or physically) in an N limited environment when the catchment is relatively dry or (2) inaccurate characterization of the high spatial and seasonal variability of inorganic N deposition in mountainous regions due to varying slope, aspect, elevation, and N sources [*Nanus*, 2003] (Appendix A).

[66] $b_{veg}$ posterior distribution was also relatively flat across the prior distribution (Figure 7A). Though most likely a sink of watershed N, the posterior distribution indicated that the $b_{veg}$ could have been modeled as a sink or source of N at the watershed scale. This is not surprising as past studies have shown vegetation as both an N sink and N source at the watershed scale. Forest disturbance by fire or clear cutting has been shown to increase stream water $NO_3^-$ immediately following the disturbance followed by decreasing $NO_3^-$ as new growth takes over the burned/cut area [*Bormann et al.*, 1968; *Vitousek*, 1979]. Residential grass areas could be a source of N by fertilizer addition. Some types of vegetation are N fixers and can be a

significant source of ecosystem $NO_3^-$ [*Postage*, 1998]. Even within non-N fixers, there is variability in the amount of $NO_3^-$ exported from different types of vegetation [*Lovett et al.*, 2002]. Aside from vegetation type, vegetation age can greatly influence stream water $NO_3^-$ export. Early to midsuccessional N limited forests retain N strongly, while older stands are less retentive of N most likely because of lower productivity rates [*Vitousek and Reiners*, 1975; *Goodale and Aber*, 2001].

[67] As demonstrated above, modeled stream water $NO_3^-$ export was highly sensitive to some model parameters (e.g., $b_{ww}$, $b_\alpha$) and less sensitive to others (e.g., $b_{veg}$, $b_{wd}$). We believe that there is great value in exploring model parameter sensitivities to understand system behavior. Although the modeled parameters and their sensitivities may be completely different in other locations, the methods and general model structure presented here may be transferable to other watersheds to explore the primary controls of $NO_3^-$ export. For example, there is no agricultural land in the West Fork watershed, however in other watersheds, agriculture may highly influence stream water $NO_3^-$ [*Omernik*, 1981] and could be added as a parameter to BiSN. Or, $b_\alpha$ may not be influential in a watershed where hydrologic flow paths are not well represented by topography (e.g., watershed with poorly drained soils, confined aquifers, or groundwater in fractured bedrock). Parameter sensitivities could also vary between watersheds. For example, in a watershed experiencing a higher level of N enrichment than the West Fork watershed, there could be increased model sensitivity to N loading from $b_s$ or $b_{wd}$ [*Aber et al.*, 1998].

### 5.3. Spatial Distribution of $NO_3^-$ Loading, Retention, and Export Across Land Use/Land Cover and Landscape Positions

[68] Spatial patterns in N loading (Figures 8A, 7C, and Table 3), upland export (Figures 8B, 8D, and Table 4), and retention (Figures 9A, 9B, and Table 4) provided insight into the relative importance of hydrologic and biological processes influencing stream water $NO_3^-$ export in the West Fork watershed. For most reach contributing areas in West Fork watershed, terrestrial storage release was the main source of $NO_3^-$ exported from the upland areas (Figure 8B). These results support other studies that have shown the majority of stream water is derived from catchment soils in the West Fork watershed (Gardner and McGlynn, manuscript in preparation, 2011) and watersheds in other regions of the U.S. [*Spoelstra et al.*, 2001; *Burns and Kendall*, 2002; *Campbell et al.*, 2002; *McHale et al.*, 2002; *Sickman et al.*, 2003; *Ohte*, 2004; *Sebestyen et al.*, 2008]. Upland $NO_3^-$ export was greatest from the South Fork and West Fork; however, the $NO_3^-$ source was different in each case. Terrestrial storage release contributed to the relatively high levels of $NO_3^-$ export in the South Fork, where a significant portion of the watershed contains surface minerals that released elevated levels of $NO_3^-$ in laboratory experiments (Ackerman-Montross et al., manuscript in preparation, 2011) that may contribute to N enriched soils. On the other hand, in the upper West Fork, wastewater inputs were the main source of stream water $NO_3^-$ export (Figure 8D and Table 4). Downstream of the South Fork confluence in the lower West Fork, the source of stream water $NO_3^-$ was an equal mixture of terrestrial storage release and wastewater $NO_3^-$.

[69] These high contributions of wastewater $NO_3^-$ to the Upper West Fork suggest that the spatial location and pattern of anthropogenic N loading may have ramifications on the magnitude and patterns of stream water $NO_3^-$ export. Smaller amounts of wastewater inputs occurring in watershed areas with short travel times to the stream had disproportionately large impacts on watershed nitrate ($NO_3^-$) export compared to larger N inputs from spatially distributed N (atmospheric deposition) or localized N inputs in watershed areas with longer travel times (septic systems). Even though atmospheric deposition and septic inputs are significantly greater than wastewater effluent export (Figure 8C), longer travel times and dispersal of N loads may allow for the majority of septic and atmospheric N to be immobilized along hydrological flow paths to the stream (Figure 8D). Conversely, wastewater N applied to a large contiguous area with short transit times to the stream may surpass the ecosystem's ability to cycle N. Consequently, much of the wastewater $NO_3^-$ is readily transported to the stream and manifests itself in higher levels of stream water $NO_3^-$ export (Figure 8D).

[70] Upland retention occurring from biological immobilization or a lack of hydrologic connectivity was by far the largest $NO_3^-$ sink in the West Fork watershed (Figure 9A, Table 4) removing 98%–99% (59.4 kg $ha^{-1}$ $yr^{-1}$) of N loading across the watershed. This high percentage of retention suggests that during the summer growing season (1) the West Fork watershed is highly N limited and/or (2) there is limited hydrologic connection between N source areas and the stream. There is an abundance of evidence that N is the most limiting nutrient for growth in most terrestrial systems [*Vitousek and Howarth*, 1995]. N inputs to an N limited system are quickly immobilized by biota [*Gundersen et al.*, 1995]. The retention rate in the West Fork seems reasonable for an N limited system during the summer growing season when biological activity peaks. For example, in other N enriched watersheds in the eastern United States and Northern Europe watershed retention on an annual basis have been shown to vary between 95% and 100% of total N inputs [*Gundersen et al.*, 1995; *Magill et al.*, 1996].

[71] Aside from biological retention, $NO_3^-$ may be retained in the uplands because of limited hydrological connectivity between the uplands and the stream. Others have shown that a hydrologic connection exists for only small fraction of the year during snowmelt or large rain events [*McGlynn and McDonnell*, 2003; *Jencso et al.*, 2009]. This seasonal timing of hydrologic connectivity may drive seasonal patterns of nutrient export exhibited in the West Fork watershed [*Pacific et al.*, 2010; *Jencso et al.*, 2010; Gardner and McGlynn, manuscript in preparation, 2011]. In other systems, where a hydrologic connection occurs for longer periods during the year, there is potential for anthropogenic N loading to have more severe impacts on stream water quality [*Ocampo et al.*, 2006].

[72] Removing upland retention from the retention plots provided insight into the relative importance of $NO_3^-$ retention in stream and riparian areas (Figure 9B and Table 4). Across the West Fork, variation in the LULC and watershed characteristics most likely drove spatial heterogeneity present in both the magnitude and relative importance of riparian and $NO_3^-$ retention. Variability in riparian buffering is

described in section 5.2. Spatial heterogeneity of instream retention could result from variability in (1) stream water $NO_3^-$ concentrations [*Earl et al.*, 2006], (2) seasonal factors (i.e., sunlight availability or temperature) [*McNamara*, 2010], (3) discharge [*Valett et al.*, 1996], and (4) groundwater-surface water exchange [*Triska*, 1989b]. BiSN's generalization of riparian and instream retention that does not account for all of these factors may be responsible for the spatial heterogeneity in riparian and instream retention of watershed N.

[73] Despite this spatial heterogeneity, patterns in the relative magnitude of riparian and instream N retention are apparent (Figure 9B and Table 4). For example, in the headwaters of the South Fork, instream processes generally immobilized more $NO_3^-$ than the riparian areas, while in the West Fork (Middle Fork, Beehive, and North Fork) more $NO_3^-$ was removed in the riparian areas than in instream processes. There are two plausible explanations for this phenomenon. First the South Fork generally has incised stream channels and limited riparian areas thus decreasing potential for retention in the riparian areas [*McGlynn and Seibert*, 2003; *Vidon and Hill*, 2006; *Jencso et al.*, 2010]. Second, the riparian and instream areas located in the headwaters of the South Fork received considerably greater N loads than the headwaters of the West Fork, primarily from mineral weathering (Ackerman-Montross et al., manuscript in preparation, 2011). Research has shown the increasing N retention with increasing N concentration [*Earl et al.*, 2006; *Covino et al.*, 2010a, 2010b].

[74] Another interesting spatial pattern across the West Fork watershed was the increasing importance of instream $NO_3^-$ retention moving downstream in the stream network. Although some research has documented the importance of lower order streams in instream retention [*Alexander et al.*, 2000; *Peterson et al.*, 2001], others have shown larger order streams playing a larger role in overall watershed N retention because of the increased opportunity for N retention [*Mulholland et al.*, 2008; *Covino et al.*, 2010a, 2010b; *McNamara*, 2010].

[75] Finally, there are a few stream reaches with a notably large percentage of N export (Table 4). Stream water N export from MFHW1 was exceptionally large: 64% of $NO_3^-$ transported from the uplands was exported from the stream. This site had the highest $NO_3^-$ loading from septic systems (9.36 kg $ha^{-1}$ $yr^{-1}$), which may be overwhelming the watershed's ability to retain $NO_3^-$. Confounding the problem, this site drains Lone Mountain, which is an alpine environment above tree line with steep slopes, consisting mainly of talus and scree. Other research has noted increased $NO_3^-$ export from talus and scree despite the potential for substantial biogeochemical processing of atmospheric $NO_3^-$ to occur in these environments [*Campbell et al.*, 2000]. Downstream from MFHW1, $NO_3^-$ export gradually decreased until the Middle Fork joins the North Fork (Figure 1) forming the West Fork, where there is a rise in stream water $NO_3^-$ export after traveling through the Big Sky Golf Course at UWF (Table 4).

## 6. Conclusion

[76] This research introduced BiSN, a modified nitrogen export coefficient model, to identify primary drivers in watershed $NO_3^-$ export and to explore the spatial patterns of N loading, export, and the relative magnitudes of terrestrial and instream retention across a developing mountain watershed. Export coefficient models can be an attractive modeling approach due to limited data requirements and applicability to land use and management practices.

[77] Bayesian MCMC methods estimated model parameters and were extremely useful in assessing model and parameter uncertainty and advancing understanding of the primary processes governing watershed $NO_3^-$ export. Modeled parameter posterior distributions identified wastewater loading and relative travel time, which represents the hydrologic transport time between N inputs and the stream channel, as being the most important controls on watershed $NO_3^-$ export. These results highlight the importance of (1) the spatial location of N loading and (2) localized N loading versus spatially distributed N loading. This implies that not all anthropogenic N loading equally impacts stream $NO_3^-$ concentrations and export. Localized N loading occurring in watershed areas with fast travel times to the stream may have a disproportionately large effect on water quality. Under these conditions, the systems ability to retain $NO_3^-$ is overwhelmed, resulting in excess $NO_3^-$ readily exported from the system.

[78] Spatial patterns in the relative magnitude of watershed retention processes revealed most watershed $NO_3^-$ retention during the summer growing season occurred in the uplands. Excluding upland retention, our results show the increasing role of instream retention with increasing N loading going downstream in the stream network. The modeling approach used here can be adapted for other watersheds to increase understanding of the primary drivers of watershed $NO_3^-$ export and to examine the spatial variability of watershed N loading, retention and export so that land managers can work effectively to minimize N loading impacts on surface waters.

## Appendix A

### A1. Big Sky Nitrogen Export Model (BiSN) Atmospheric Deposition Calculation

[79] Precipitation in the drainage varies significantly across elevation gradients; annual precipitation exceeds 1270 mm at higher elevations (3400 m) and is less than 500 mm near the watershed outlet (1800 m). The West Fork watershed has two year round weather stations, which measure precipitation (Figure 1B): (1) the Lone Mountain SNOTEL station is located in Bear Basin in the headwaters of the North Fork at 2706 m in a subalpine environment and (2) the Lone Mountain Ranch station located in the valley bottom at 2100 m. There were six years that both stations recorded data (2002–2007). Linear regression developed a relationship between average annual precipitation and elevation. This relationship was used to scale precipitation. Calibrated wet N deposition concentration was multiplied by precipitation to calculate wet deposition N loading for each grid cell.

### A2. BiSN Instream Nitrogen Decay

[80] Multiple regression determined the relationship between measured instream areal retention (g $m^{-2}$ $d^{-1}$) of

$NO_3^-$ and potential explanatory variables. Potential explanatory variables to predict areal retention included watershed area, nitrate concentration, and stream order. Watershed area and stream order for each reach was determined through terrain analysis and measured $NO_3^-$ concentration. A significant linear relationship ($R^2 = 0.74$) was found between areal retention, watershed area, and measured stream water $NO_3^-$. Instream areal $NO_3^-$ retention increased with watershed area and $NO_3^-$ concentration.

[81] BiSN (equations (1)) computes areal $NO_3^-$ retention for each stream reach by applying the regression relationship between watershed area and nitrate concentration. The computed areal retention was multiplied by the reach length (m) and reach width (m) to determine total N immobilization (kg $d^{-1}$). The upland N load from the incremental subwatershed $i$ (Figure 3) was assumed to travel on average half the reach length. Therefore, stream *decay* function was applied for only half the distance of stream reach $i$:

$$\text{Upland Load} - (0.5 * \text{reach length}_i * \text{reach width}_i * \textit{decay}). \quad \text{(A1)}$$

[82] For the upstream load (**$NE_{up}$**), N immobilization (*decay*) occurs throughout the entire length of the downstream reach $i$:

$$\mathbf{NE_{up}} - (\text{reach length}_i * \text{reach width}_i * \textit{decay}). \quad \text{(A2)}$$

[83] Stream width assumptions in (A1) and (A2) were dependent on stream order. Based on field observations, a first, second, third, and fourth order streams were assumed to have a stream width of 1, 2, 4, and 8 m, respectively.

[84] **Acknowledgments.** Financial support was provided by the Environmental Protections Agency (EPA) STAR grant R832449, EPA 319 funds administered by the MT Department of Environmental Quality, the U.S. National Science Foundation BCS 0518429, and the USGS 104(b) grant Program administered by the MT Water Center. K.K.G. acknowledges support from the EPA STAR Fellowship and NSF GK-12 Fellowship programs. Special thanks to G. Ackerman for laboratory analyses, field support, and parallel and supportive research related to the rock weathering experiments.

## References

Aber, J. D., K. J. Nadelhoffer, P. Steudler, and J. M. Melillo (1989), Nitrogen saturation in northern forest ecosystems: Excess nitrogen from fossil fuel combustion may stress the biosphere, *BioScience*, *39*(6), 378–385.

Alexander, R. B., R. A. Smith, G. E. Schwarz, E. W. Boyer, J. V. Nolan, and J. W. Brakebill (2008), Differences in phosphorus and nitrogen delivery to the Gulf of Mexico from the Mississippi River Basin, *Environ. Sci. Technol.*, *42*, 822–830.

Alexander, R. B., P. J. Johnes, E. W. Boyer, and R. A. Smith (2002), A comparison of models for estimating the riverine export of nitrogen from large watersheds, *Biogeochemistry*, *57*, 295–339.

Allen, J. D. (1995), *Stream Ecology, Structure and Function of Running Waters*, Kluwer, Dordrecht, The Netherlands.

Alt, D., and D. W. Hyndman (1986), *Roadside Geology of Montana*, Mountain Press, Missoula, MT.

Baron, J. S., D. S. Ojima, and E. A. Holland (1994), Analysis of nitrogen saturation potential in Rocky-Mountain tundra and forest—Implications for aquatic system, *Biogeochemistry*, *27*(10), 61–82.

Bates, B. C., and E. P. Campbell (2001), A Markov chain Monte Carlo scheme for parameter estimation and inference in conceptual rainfall-runoff modeling, *Water Resour. Res.*, *37*(4), 937–947, doi:10.1029/2000WR900363.

Beaulac, M. N., and K. M. Reckhow (1982), An examination of land use-nutrient export relationships, *Water Resour. Bull.*, *18*, 1013–1024.

Beck, M. B. (1987), Water quality modeling: A review of the analysis of uncertainty, *Water Resour. Res.*, *23*(8), 1393–1442, doi:10.1029/WR023i008p01393.

Beven, K. (2006), A manifesto for the equifinality thesis, *J. Hydrol.*, *320*, 18–36.

Beven, K. J. (2001), *Rainfall-Runoff Modelling, The Primer*, John Wiley, West Sussex, England.

Beven, K. (1993), Prophecy, reality and uncertainty in distributed hydrological modeling, *Adv. Water Resour.*, *16*, 41–51, doi:10.1016/0309-708(93)90028-E.

Beven, K. J., and M. J. Kirkby (1979), A physically-based variable contributing area model of basin hydrology, *Hydrol. Sci. Bull.*, *24*(1), 43–69.

Bohlke, J. K., and J. M. Denver (1995), Combined use of groundwater dating, chemical, and isotopic analyses to resolve the history and fate of nitrate contamination in two agricultural watersheds, Atlantic coastal plain, Maryland, *Water Resour. Res.*, *31*(9), 2319–2339, doi:10.1029/95WR01584.

Bormann, F. H., G. E. Likens, D. W. Fisher, and R. S. Pierce (1968), Nutrient loss accelerated by clear-cutting of a forest ecosystem, *Science*, *159*(3817), 882–884.

Bormann, F. H., G. E. Likens, and J. M. Melillo (1977), Nitrogen budget for an aggrading northern hardwood forest ecosystem, *Science*, *196*, 981–983.

Brooks, P. D., M. W. Williams, S. K. Schmidt (1996), Microbial activity under alpine snowpacks, Niwot Ridge, Colorado, *Biogeochemistry*, *32*(2), 93–113.

Brunet, R. C., and L. J. Garcia-Gil (1996), Sulfide-induced dissimilatory nitrate reduction to ammonia in anaerobic freshwater sediments, *FEMS Microbiol. Ecol.*, *21*, 131–138.

Burns, D. A. (2003), Atmospheric nitrogen deposition in the Rocky Mountains of Colorado and southern Wyoming—A review and new analysis of past study results, *Atmos. Environ.*, *37*(7), 921–932.

Burns, D. A., and C. Kendall (2002), Analysis of $\delta^{18}O$ and $\delta^{15}N$ to differentiate $NO_3^-$ sources in runoff at two watersheds in the Catskill Mountains of New York, *Water Resour. Res.*, *38*(5), 1051, doi:10.1029/2001WR000292.

Burt, T. P., L. S. Matchett, K. W. T. Goulding, C. P. Webster, and N. E. Haycock (1999), Denitrification in riparian buffer zones: The role of floodplain hydrology, *Hydrol. Processes*, *13*, 1451–1463.

Campbell, D. H., J. S. Baron, K. A. Tonnessen, P. D. Brooks, and P. F. Schuster (2000), Controls on nitrogen flux in alpine/subalpine watersheds of Colorado, *Water Resour. Res.*, *36*, 37–47.

Campbell, D. H., C. Kendall, C. C. Y. Chang, S. R. Silva, and K. A. Tonnessen (2002), Pathways for nitrate release from an alpine watershed: Determination using $d^{15}N$ and $d^{18}O$, *Water Resour. Res.*, *38*(5), 1052–1071, 1052, doi:10.1029/2001WR000294.

Campos, N., R. Lawrence, B. L. McGlynn, and K. K. Gardner (2010), Effects of Lidar-QuickBird fusion on object oriented classification of mountain resort development, *J. Appl. Remote Sensing*, *4*, 043556. doi:10.1117/1.3519370.

Carle, M. V., P. N. Halpin, and C. A. Stow (2005), Patterns of watershed urbanization and impacts on water quality, *J. Am. Water Resour. Assoc.*, *41*(3), 693–708.

Chang, C. C. Y., C. Kendall, S. R. Silva, W. A. Battaglin, and D. H. Campbell (2002), Nitrate stable isotopes: Tools for determining nitrate sources among different land uses in the Mississippi River Basin, *Groundwater*, *59*, 1874–1885.

Cleveland, C. C., et al. (1999), Global patterns of terrestrial biological nitrogen ($N_2$) fixation in natural ecosystems, *Global Biogeochem. Cycles*, *13*(2), 623–645.

Colman, J. A., J. P. Masterson, W. J. Pabich, and D. A. Walter (2004), Effects of aquifer travel time on nitrogen transport to a coastal embayment, *Groundwater*, *42*(7), 1069–1078.

Covino, T. P., B. L. McGlynn, and R. A. McNamara (2010a), Tracer additions for spiraling curve characterization (TASCC): Quantifying stream nutrient uptake kinetics from ambient to saturation, *Limnol. Oceanogr. Methods*, doi:10:4319/lom.2010.8.484.

Covino, T. P., B. L. McGlynn, and M. A. Baker (2010b), Separating physical and biological nutrient retention and quantifying uptake kinetics from ambient to saturation in successive mountain stream reaches, *J. Geophys. Res.* Biogeosci., *115*, G04010, doi:10.1029/2009JG001263.

Cressie, N (1993). *Statistics for Spatial Data*, John Wiley, New York.

Davidson, E. A., J. Chorover, and D. B. Dail (2003), A mechanism of abiotic immobilization of nitrate in forest ecosystems: The ferrous wheel hypothesis, *Global Change Biol.*, *9*, 228–236.

Dent, C. L., N. B. Grimm, E. Marti, J. W. Edmonds, J. C. Henry, and J. R. Welter (2007), Variability in surface-subsurface hydrologic interactions and implications for nutrient retention in an arid-land stream, *J. Geophys. Res.*, *112*, G04004, doi:10.1029/2007JG000467.

Dent, C. L., and N. B. Grimm (1999), Spatial heterogeneity of stream water nutrient concentrations over successional time, *Ecology*, *80*, 2283–2298.

Dietz, M. E., and J. C. Clausen (2008), Stormwater runoff and export changes with development in a traditional and low impact subdivision, *J. Environ. Manage.*, *87*, 560–566.

Dunne, T. (1978), Field studies of hillslope processes, in *Hillslope Hydrology*, edited by M. J. Kirkby, John Wiley, New York, 227–289.

Earl, S. R., H. M. Valett, and J. R. Webster. (2006), Nitrogen saturation in streams, *Ecology*, *87*(12), 3140–3151.

Edreny, T. A., and E. F. Wood (2003), Watershed weighting of export coefficients to map critical phosphorous loading areas, *J. Am. Water Resour. Assoc.*, *39*(1), 165–181.

Edwards, R. (2007), personal communications.

Fahey, T. J., J. B. Yavitt, J. A. Pearson, and D. H. Knight, (1985), The nitrogen cycle in lodgepole pine forests, southeastern Wyoming, *Biogeochemistry*, *1*(3), 257–275.

Fisk, M. C., and S. K. Schmidt (1995), Nitrogen mineralization and microbial biomass N dynamics in three alpine tundra communities, *Soil Sci. Soc. Am. J.*, *59*, 1036–1043.

Fraterrigo, J. M., and J. A. Downing (2008), The influence of land use on lake nutrients varies with watershed transport capacity, *Ecosystems*, *11*, 1021–1034.

Gardner, K. K., and B. L. McGlynn (2009), Seasonality in spatial variability and influence of land use/land cover and watershed characteristics on streamwater nitrate concentrations in the Northern Rocky Mountains, *Water Resour. Res.*, *45*, W08411, doi:10.1029/2008WR007029.

Gelman, A., and D. B. Rubin (1992), Inference from iterative simulation using multiple sequences, *Stat. Sci.*, *7*, 457–511.

Gelman, A., J. B. Carlin, H. S. Stern, and D. B. Rubin (2004), *Bayesian Data Analysis*, 2nd ed., Chapman and Hall, New York.

Goodale, C. L., and J. D. Aber (2001), The long-term effects of land-use history on nitrogen cycling in northern hardwood forests, *Ecol. Appl.*, *11*(1), 253–267.

Grabs, T., K. J. Jencso, B. L. McGlynn, and J. Seibert (2010), Calculating terrain indices along streams—A new method for separating stream sides, *Water Resour. Res.*, *46*, W12536, doi:10.1029/2010WR009296.

Griffin, C. B. (1995), Uncertainty analysis of BMP effectiveness for controlling nitrogen from urban nonpoint sources, *Water Resour. Bull.*, *31*(6), 1041–1050.

Grimm, N. B., and K. C. Petrone (1997), Nitrogen fixation in a desert stream ecosystem, *Biogeochemistry*, *37*, 33–61.

Groffman, P. M., C. T. Driscoll, T. J. Fahey, J. P. Hardy, R. D. Fitzhugh, and G. L. Tierney (2001), Effects of mild winter freezing on soil nitrogen and carbon dynamics in a northern hardwood forest, *Biogeochemistry*, *56*, 191–213.

Gundersen, P., and L. Rasmussen (1995), Nitrogen mobility in a nitrogen limited forest at Klosterhede, Denmark, examined by $NH_4NO_3$ addition, *For. Ecol. Manage.*, *71*, 75–58.

Haario, H., E. Saksman, and J. Tamminen (2001), An adaptive Metropolis algorithm, *Bernoulli*, *7*(2), 223–242.

Hadas, A., M. Sofer, J. A. E. Molina, P. Barak, and C. E. Clapp (1992), Assimilation of nitrogen by soil microbial population: $NH_4$ versus organic N, *Soil Biol. Biochem.*, *24*, 137–143.

Hanrahan, G., M. Gledhill, W. A. House, and P. J. Worsfold (2001), P loading in the Frome catchment, UK: Seasonal refinement of the coefficient modeling approach, *J. Environ. Qual.*, *30*(5), 1738–1746.

Hart, S. C., and M. K. Firestone (1991), Forest-mineral soil interactions in the internal nitrogen cycle of an old-growth forest, *Biogeochemistry*, *12*(2), 103–127.

Hassan, A. E., H. M. Bekhit, and J. B. Chapman (2009), Using Markov chain Monte Carlo to quantify parameter uncertainty and its effect on predictions of a groundwater flow model, *Environ. Model. Software*, *24*, 749–763.

Hession, W. C., and D. E. Storm (2000), Watershed-level uncertainties: Implications for phosphorus management and eutrophication, *J. Environ. Qual.*, *29*(4), 1172–1179.

Hill, A. R. (1996), Nitrate removal in stream riparian zones, *J. Environ. Qual.*, *25*, 743–755.

Holloway, J. M., R. A. Dahlgren, and W. H. Casey (2001), Nitrogen release from rock and soil under simulated field conditions, *Chem. Geol.*, *174*, 403–413.

Holloway, J. M., R. A. Dahlgren, B. Hansen, and W. H. Casey (1998), Contribution of bedrock nitrogen to high nitrate concentrations in stream-water, *Nature*, *395*, 785–788.

Hong, B., D. P. Saney, P. B. Woodbury, and D. A. Weinstein (2004), Long-term nitrate export pattern from Hubbard Brook 6 watershed driven by climatic variation, *Water Air Soil Pollution*, *160*, 293–326.

Jacot, K. A., A. Luscher, J. Nosberger, and U. A. Hartwig (2000), The relative contribution of symbiotic N2 fixation and other nitrogen sources to grassland ecosystems along an altitudinal gradient in the Alps, *Plant Soil*, *225*, 201–211.

Janssen, B. H. (1996), Nitrogen mineralization in relation to C:N ratio and decomposability of organic materials, *Plant Soil*, *181*, 39–45.

Jencso, K. J., B. L. McGlynn, M. N. Gooseff, S. M. Wondzell, and K. E. Bencala (2009), Hydrologic connectivity between landscapes and streams: Transferring reach and plot scale understanding to the catchment scale, *Water Resour. Res.*, *45*, W04428, doi:10.1029/2008WR007225.

Jencso, K. J., B. L. McGlynn, M. N. Gooseff, K. E. Bencala, and S. M. Wondzell (2010), Hillslope hydrologic connectivity controls riparian groundwater turnover: Implications of catchment structure for riparian buffering and stream water sources, *Water Resour. Res.*, W10524, doi:10.1029/2009WR008818.

Johnes, P. J. (1996), Evaluation and management of the impact of land use change on the nitrogen and phosphorus load delivered to surface waters: The export coefficient modeling approach, *J. Hydrol.*, *183*, 323–349.

Johnes, P. J., and A. L. Heathwaite (1997), Modeling the impact of land use change on water quality in agricultural catchments, *Hydrol. Processes*, *11*, 269–286.

Kellog, K. S., and V. S. Williams (2005). Geologic Map of the Ennis 30′ × 60′ Quadrangle, Madison and Gallatin counties, Montana and Park County, Wyoming. Montana Bureau of Mines and Geology Open File No. 529.

Khadam, I. M., and J. J. Kaluarachchi (2006), Water quality modeling under hydrologic variability and parameter uncertainty using erosion-scaled export coefficients, *J. Hydrol.*, *330*, 354–367.

Kirchner, J. W. (2006), Getting the right answers for the right reasons: Linking measurements, analyses, and models to advance the science of hydrology, *Water Resour. Res.*, *42*, W03S04, doi:10.1029/2005WR004362.

Lawrence, G. B., G. M. Lovett, and Y. H. Baevsky (2000), Atmospheric deposition and watershed nitrogen export along an elevational gradient in the Catskill Mountains, New York, *Biogeochemistry*, *50*, 21–43.

Likens, G. E., F. H. Bormann, N. M. Johnson, D. W. Fisher, and R. S. Pierce (1970), Effects of forest cutting and herbicide treatment on nutrient budgets in the Hubbard Brook watershed-ecosystem, *Ecolog. Mono.*, *40*(1), 23–47.

Lovett, G. M., K. C. Weathers, and M. A. Arthur (2002), Control of nitrogen loss from forested watersheds by soil carbon:nitrogen ratio and tree species composition, *Ecosystems*, *5*, 712–718.

Lovett, G. M., J. J. Bowser, and E. S. Edgerton (1997), Atmospheric deposition to watersheds in complex terrain, *Hydrol. Processes*, *11*, 645–655.

Lowrance, R., R. Todd, J. Fail Jr., O. Hendrickson Jr., R. Leonard, and L. Asmussen (1984), Riparian forests as nutrient filters in agricultural watersheds, *Bioscience*, *34*, 374–377.

Lunetta, R. S., R. G. Greene, and J. G. Lyon (2005), Modeling the distribution of diffuse nitrogen sources and sinks in the Neuse River Basin of North Caroline, USA, *J. Am. Water Resour. Assoc.*, *41*(5), 1129–1147.

Luo, Y., E. Weng, X. Wu, C. Gao, Z. Zhou, and L. Zhang (2009), Parameter identifiability, constraint, and equifinality in data assimilation with ecosystem models, *Ecol. Appl.*, *19*(3), 571–574.

Magill, A. H., M. R. Downs, K. J. Nadelhoffer, R. A. Hallet, and J. D. Aber (1996), Forest ecosystem response to four years of chronic nitrate and sulfate additions at Bear Brooks Watershed, Maine, USA, *For. Ecol. Manage.*, *84*, 29–37.

Maitre, V., A. Cosandey, E. Desagher, and P. Parriaux (2003), Effectiveness of groundwater nitrate removal in a river riparian area: The importance of hydrogeological conditions, *J. Hydrol.*, *278*(1–4), 76–93.

Marshall, L., D. Nott, and A. Sharma (2004), A comparative study of Markov chain Monte Carlo methods for conceptual rainfall-runoff modeling, *Water Resour. Res.*, *40*, W02501, doi:10.1029/2003WR002378.

McFarland, A. M. S., and L. M. Hauck (2001), Determining nutrient export coefficients and source loading uncertainty using in-stream monitoring data, *J. Am. Water Resour. Assoc.*, *37*(1), 223–236.

McGlynn, B. L. (2005), The role of riparian zones in steep mountain watersheds, in *Global Change and Mountain Regions*, Advances in Global Change Research book series, edited by M. Beniston, Kluwer, Dordrecht, The Netherlands.

McGlynn, B. L., and J. J. McDonnell (2003), Quantifying the relative contributions of riparian and hillslope zones to catchment runoff and composition, *Water Resour. Res.*, *39*(11), 1310, doi:10.1029/2003WR002091.

McGlynn, B. L., and J. Seibert (2003), Distributed assessment of contributing area and riparian buffering along stream networks, *Water Resour. Res.*, *39*(4), 1082, doi:10.1029/2002WR001521.

McGuire, K. J., J. J. McDonnell, M. Weiler, C. Kendall, B. L. McGlynn, J. M. Welker, and J. Seibert (2005), The role of topography on catchment-scale water residence time, *Water Resour. Res.*, *41*, W05002, doi:10.1029/2004WR003657.

McHale, M. R., J. J. McDonnell, M. J. Mitchell, and C. Cirmo (2002), A field based study of soil and groundwater nitrate release in an Adirondack forested watershed, *Water Resour. Res.*, *38*(4), 1029–1038, 1031, doi:10.1029/2000WR000102.

McNamara, R. A. (2010), Stream nitrogen uptake dynamics from ambient to saturation across development gradients, stream network position, and seasons, Master Thesis, Montana State University, Bozeman, Montana.

Meile, C., W. P. Porubsky, R. L. Walker, and K. Payne (2010), Natural attenuation of nitrogen loading from septic effluents: Spatial and environmental controls, *Water Res.*, *44*, 1399–1208.

Meyer, J. L., M. J. Pal, and W. K. Taulbee (2005), Phosphorous nitrogen, and organic carbon flux in a headwater stream, *Achiv. Hydrobiol.*, *91*, 28–44.

Meyer, J. L., G. E. Likens, and J. Sloane (1981), Phosphorus, nitrogen and organic carbon flux in a headwater stream ecosystem, *Archiv fur Hydrobiologie*, *91*, 28–44.

Miller, A. E., J. P. Schimel, J. O. Sickman, K. Skeen, T. Meixner, and J. M. Melack (2009), Seasonal variation in nitrogen uptake and turnover in two high-elevation soils: Mineralization responses are site-dependent, *Biogeochemistry*, *93*, 253–270.

Mulholland, P. J., et al. (2008), Stream denitrification across biomes and its response to anthropogenic nitrate loading, *Nature*, *452*(13), doi:10.1038/nature06686.

Nadelhoffer, K. J., M. R. Downs, and B. R. Fry (1999), Sinks for 15N-enriched additions to an oak forest and a red pine plantation, *Ecol. Appl.*, *9*, 72–86.

Nanus, L., D. H. Campbell, G. P. Ingersoll, D. W. Clow, and M. A. Mast (2003), Atmospheric deposition maps for the Rocky Mountains, *Atmos. Environ.*, *37*, 4881–492.

National Atmospheric Deposition Program (NADP) (2010), http://nadp.sws.uiuc.edu/, NADP Program Office, Illinois State Water Survey, Champaign, IL.

National Science Foundation (NSF) (1976), Impacts of large recreational development upon semi-primitive environments, NSF RANN Program Final Report.

Newson, M. D. (1997), *Land, Water and Development: Sustainable Management of River Basin Systems*, Routledge, London.

Ocampo, C. J., M. Sivapalan, and C. E. Oldham (2006), Hydrological connectivity of upland-riparian zones in agricultural catchments: Implications for runoff generation and nitrate transport, *J. Hydrol.*, *331*, 643–658.

Ohte, N., S. D. Sebestyen, J. B. Shanley, D. H. Doctor, C. Kendall, S. D. Wankel, and E. W. Boyer (2004), Tracing sources of nitrate in snowmelt runoff using a high-resolution isotopic technique, *Geophys. Res. Lett.*, *31*, L21506, doi:10.1029/2004GL020908.

Omernik, J. M., A. R. Abernathy, and L. M. Male (1981), Stream nutrient levels and proximity of agricultural and forest land to streams: Some relationships, *J. Soil Water Conserv.*, *36*(4), 227–231.

Pacific, V., K. Jencso, and B. L. McGlynn (2010), Variable flushing mechanisms and landscape structure control stream DOC export during snowmelt in a set of nested catchments, *Biogeochemistry*, doi:10.1007/s10533-009-9401-1.

Perrin, C., C. Michel, V. Andreassian (2001), Does a large number of parameters enhance model performance? Comparative assessment of common catchment model structures on 429 catchments, *J. Hydrol.*, *242*, 275–310.

Peterson, E. E., A. A. Merton, D. M. Theobald, and N. S. Urquhart (2006), Patterns of spatial autocorrelation in stream water chemistry, *Environ. Monitor. Assess.*, *121*(1), 569–594.

PBS&J, Inc. (2005), 2005 Biological monitoring Chlorophyll a data summary upper Gallatin water quality restoration planning areas, TMDL Report prepared for the Montana Department of Environmental Quality.

PBS&J, Inc. (2008), West Fork Gallatin River streamflow study 2007–2008, TMDL Report prepared for the Montana Department of Environmental Quality.

Post, W. M., J. Pastor, P. J. Zinke, and A. G. Stangenberger (1985), Global patterns of soil nitrogen storage, *Nature*, *317*(17), 613–616.

Postage, J. (1998), *Nitrogen Fixation.* 3rd ed., Cambridge University Press, Cambridge.

Qian, S. S., K. H. Reckhow, J. Zhai, and G. McMahon (2005), Nonlinear regression modeling of nutrient loads in streams: A Bayesian approach, *Water Resour. Res.*, *41*, W07012, doi:10.1029/2005WR003986.

Qualls, R. G., and B. L. Haines (1992), Biodegradability of dissolved organic matter in forest throughfall, soil solution, and streamwater, *Soil Sci. Soc. Am. J.*, *56*, 578–586.

Rast, W., and G. F. Lee (1983), Evaluation of nutrient loading estimates for lakes, *J. Environ. Eng.*, *109*, 502–517.

Ross, D. S., B. C. Wemple, A. E. Jamison, G. Fredrikesen, J. B. Shanley, G. B. Lawrence, S. W. Bailey, and J. L. Campbell (2009), A cross-site comparison of factors influencing soil nitrification rates in the Northeastern USA forested watersheds, *Ecosystems*, *12*, 158–178.

Reckhow, K. H., M. N. Beaulac, and J. T. Simpson (1980), Modeling P loading and lake response under uncertainty: A manual and compilation of export coefficients, U.S. Environmental Protection Agency Report No: EPA-440/5-80-011, Office of Water Regulations and Standards, Criteria and Standards Division, U.S. Environmental Protection Agency, Washington, DC.

Savenije, H. H. G. (2001), Equifinality, a blessing in disguise?, *Hydrol. Processes*, *15*, 2835–2838, doi:10.1002/hyp.494.

Schade, J. D., E. Marti, J. R. Welter, S. G. Fisher, and N. B. Grimm (2002), Sources of nitrogen to the riparian zone of a desert stream: Implications for riparian vegetation and nitrogen retention, *Ecosystems*, *5*, 68–69.

Seastedt, T. R., W. D. Bowman, N. Caine, D. McKnight, A. Townsend, and M. W. Williams (2004), The landscape continuum: A model for high-elevation ecosystems, *BioScience*, *54*(2), 111–120.

Sebestyen, S. D., E. W. Boyer, J. B. Shanley, C. Kendall, D. H. Doctor, G. R. Aiken, and N. Ohte (2008), Sources, transformations, and hydrological processes that control stream nitrate and dissolved organic matter concentrations during snowmelt in an upland forest, *Water Resour. Res.*, *44*, W12410, doi:10.1029/2008WR006983.

Seibert, J., and J. J. McDonnell (2002), On the dialog between experimentalist and modeler in catchment hydrology: Use of soft data for multicriteria model calibration, *Water Resour. Res.*, *38*(11), 1241, doi:10.1029/2001WR000978.

Seibert, J., and B. L. McGlynn (2007), A new triangular multiple flow-direction algorithm for computing upslope areas from gridded digital elevation models, *Water Resour. Res.*, *43*, W04501, doi:10.1029/2006WR005128.

Seitzinger, S. P., R. V. Styles, E. W. Boyer, R. B. Alexander, G. Billen, R. W. Howarth, B. Mayer, and N. Van Breemen (2002), Nitrogen retention in rivers: Model development and application to watersheds in the northeastern U.S.A., *Biogeochemistry*, *57/58*, 199–237.

Shields, C. A., L. E. Band, N. Law, P. M. Groffman, S. S. Kaushal, K. Savas, G. T. Fisher, and K. T. Belt (2008). Streamflow distribution of non-point source nitrogen export from urban-rural catchments in the Chesapeake Bay watershed, *Water Resour. Res.*, *44*, W09416, doi:10.1029/2007WR006360.

Shrestha, S., F. Kazama, and L. T. H. Newham (2008), A framework for estimating pollutant export coefficients from long-term in-stream water quality monitoring data, *Environ. Model. Software*, *23*, 182–194.

Sickman, J. O., A. Leydecker, and J. M. Melack (2003), Mechanisms underlying export of N from high-elevation catchments during seasonal transitions, *Biogeochemistry*, *64*(1), 1–24.

Smith, R. A., G. E. Schwarz, and R. B. Alexander (1997), Regional interpretation of water quality monitoring data, *Water Resour. Res.*, *33*, 2781–2798, doi:10.1029/97WR02171.

Smith, T. J., and L. A. Marshall (2010), Exploring uncertainty and model predictive performance concepts via a modular snowmelt-runoff modeling framework, *Environ. Model. Software*, *25*, 691–701.

Soulsby, C., D. Tetzlaff, S. M. Dunn, and S. Waldron (2006), Scaling up and out in runoff process understanding—Insights from nested experimental catchment studies, *Hydrol. Processes*, *20*, 2461–2465.

Spoelstra, J., S. L. Schiff, R. J. Elgood, R. G. Semkin, and D. S. Jeffries (2001), Tracing the sources of exported nitrate in the Turkey Lakes Watershed using $^{15}N/^{14}N$ and $^{18}/^{16}O$ isotopic ratios, *Ecosystems*, *4*, 536–544.

Springob, G., and H. Kirchmann (2003), Bulk soil C to N ratio as a simple measure of net N mineralization from stabilized soil organic matter in sandy arable soil, *Soil Biology Biochem.*, *35*, 629–632.

Tiedje, J. M. (1988), Ecology of denitrification and dissimilatory nitrate reduction to ammonium, in *Environmental Microbiology of Anaerobes*, edited by A. J. B. Zehnder, John Wiley and Sons, New York.

Triska, F. J., A. P. Jackman, J. H. Duff, and R. J. Avanzino (1994), Ammonium sorption to channel and riparian sediments: A transient storage pool for dissolved inorganic nitrogen, *Biogeochemistry*, *26*, 67–83.

Triska, F. J., V. C. Kennedy, R. J. Avanzino, G. W. Zellweger, and K. E. Bencala (1989a), Retention and transport of nutrients in a third-order stream: Channel processes, *Ecology*, *70*(6), 1877–1892.

Triska, F. J., V. C. Kennedy, R. J. Avanzino, G. W. Zellweger, and K. E. Bencala (1989b), Retention and transport of nutrients in a third-order stream in Northwestern California: Hyporheic processes, *Ecology*, *70*(6), 1893–1905.

Triska, F. J., J. R. Sedell, K. Cromack, S. V. Gregory, and F. M. McCorison (1984), Nitrogen budget for a small coniferous forest stream, *Ecolog. Mono.*, *54*, 119–140.

U.S. Department of Agriculture (USDA) Forest Service (FS) (1994), Ecoregions of the United States, http://www.fs.fed.us/land/pubs/ecoregions/.

U.S. Environmental Protection Agency Clean Market Air Division (USEPA CMAD) (2009), Clean Air Status and Trends Network (CASTN), http://www.epa.gov/castnet/.

U.S. EPA (2002), *Onsite Wastewater Treatment System Manual*, EPA/625/R-00/008. U.S. Environmental Protection Agency, Office of Water, Washington, DC, and Office of Research and Development, Cincinnati, OH.

U.S. EPA (1976), *Areawide Assessment Procedures Manual, Volumes I, II, and III*, EPA/600/9-76/014 (NTIS PB-271863), USEPA Office of Research and Development.

USDA Forest Service (FS) (2004), Gallatin National Forest: Streams, http://www.fs.fed.us/r1/gallatin/?page=resources/fisheries/streams.

USDA Natural Resource Conservation Service (NRCS) (2008), Snotel precipitation data, http://www.wcc.nrcs.usda.gov/cgibin/wygraph-multi.pl?stationidname=11D19S-LONE+MOUNTAIN&state=MT&wateryear=2008.

USDA S. C. S. (1978), General Soil Map, Montana, Ext. Misc. Publication No. 16.

USDA Soil Conservation Service (USDA SCS) (1982), Soils of Montana, Bulletin 744, November, Montana State University, Bozeman, MT.

Valett, H. M., J. A. Morrice, C. N. Dahm, and M. E. Campana (1996), Parent lithology, surface-groundwater exchange, and nitrate retention, *Limnol. Oceanogr.*, *41*, 333–345.

Vidon, P. G., and A. R. Hill (2006), A landscape approach to estimate riparian hydrological and nitrate removal functions, *J. Am. Water Resour. Assoc.*, *42*(4), 1099–1112.

Vitousek, P. M. (1979), Nitrate losses from disturbed forests—Patterns and mechanisms, *Science*, *25*(4), 605–619.

Vitousek, P. M., and W. A. Reiners (1975), Ecosystem succession and nutrient retention: A hypothesis, *BioScience*, *25*(6), 376–381.

Vitousek, P. M., J. Aber, R. W. Howarth, G. E. Likens, P. A. Matson, D. W. Shindler, W. H. Schlesinger, and D. G. Tilman (1997), Human alterations of the global nitrogen cycle: Sources and consequences, *Ecol. Appl.*, *7*(3), 737–750.

Vitousek, P. M., et al. (2002), Towards an ecological understanding of biological nitrogen fixation, *Biogeochemistry*, *57/58*, 1–45.

Webster, J. R., and H. M. Valett (2006), Solute dynamics, in *Methods in Stream Ecology*, edited by F. R. Hauer and G. A. Lamberti, pp.169–185, Elsevier, Burlington, MA.

Wetzel, R. G. (2001), *Limnology*, 3rd ed., Academic, San Diego.

Whitehead, P. G., P. J. Johnes, and D. Butterfield (2002), Steady state and dynamic modelling of nitrogen in River Kennet: Impacts of land use change since 1930s, *Sci. Total Environ.*, *282*, 417–434.

Wickham, J. D., and T. G. Wade (2002), Watershed level risk assessment of nitrogen and phosphorus export, *Comput. Electron. Agric.*, *37*, 15–24.

Wong, J. W. C., C. W. Y Chan, and K. C. Cheung (1998), Nitrogen and phosphorus leaching from fertilizer applied on golf course: Lysimeter study, *Wate, Air Soil Pollution*, *107*(1–4), 335–345.

Worrall, F., and T. P. Burt (1999), The impact of land-use change on water quality at the catchment scale: The use of export coefficients and structural models, *J. Hydrol.*, *221*(1–2), 75–90.

Young, P., S. Parkinson, and M. Lees (1996), Simplicity out of complexity in environmental modeling: Occam's razor revisited, *J. Appl. Stat.*, *23*(2–3), 165–210.

Zobrist, J., and P. Reichert (2006), Bayesian estimation of export coefficients from diffuse and point sources in Swiss watersheds, *J. Hydrol.*, *329*, 207–223.

K. K. Gardner, L. A. Marshall, and B. L. McGlynn, Department of Land Resources and Environmental Sciences, Montana State University, Bozeman, Montana 59717, USA. (kristin.k.gardner@gmail.com)